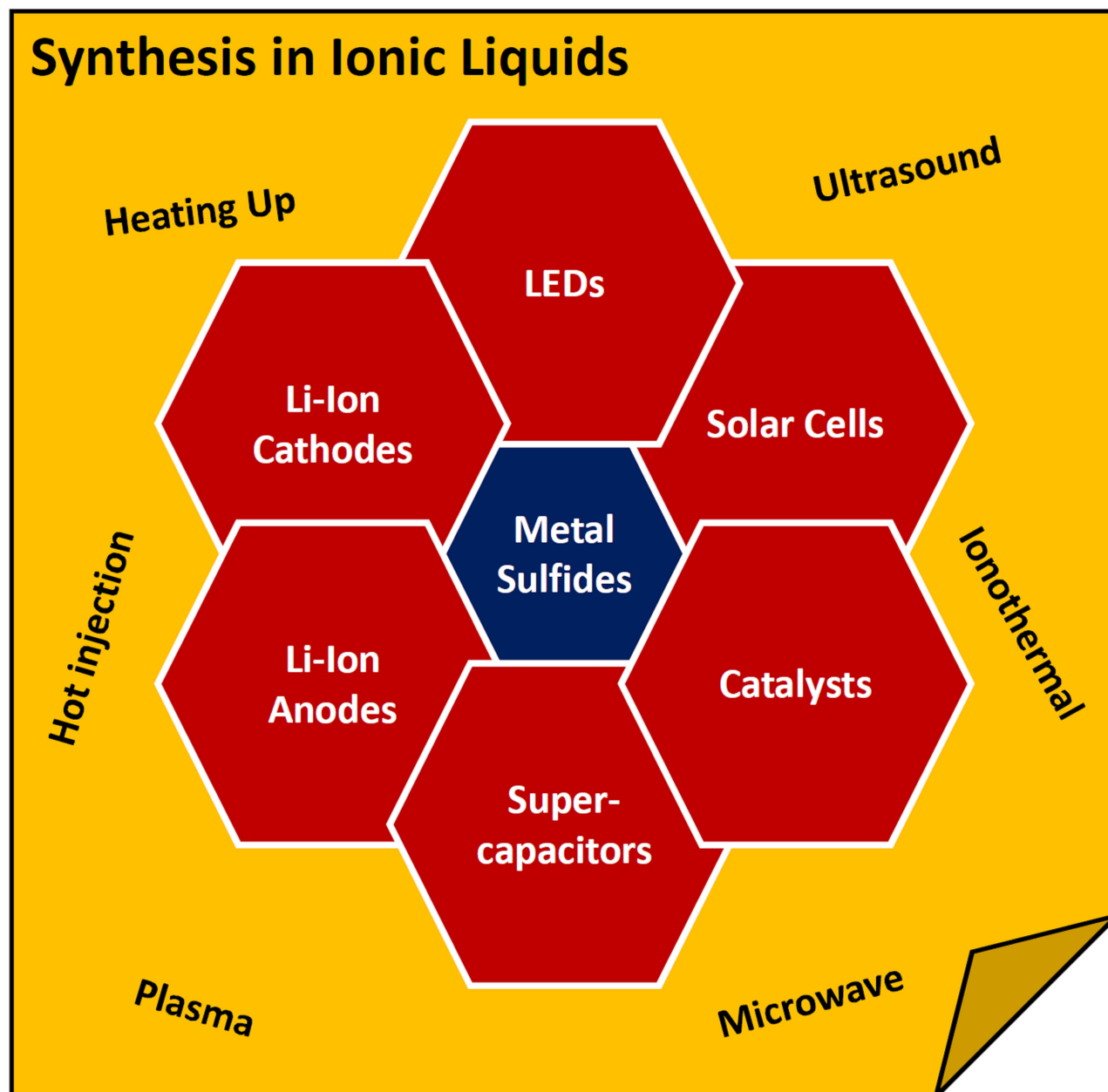


Special
Issue

Metal Sulfide Nanoparticle Synthesis with Ionic Liquids – State of the Art and Future Perspectives

Christian Balischewski^{+, [a]} Hyung-Seok Choi^{+, [b]} Karsten Behrens,^[a] Alkit Beqiraj,^[a] Thomas Körzdörfer,^[a] André Geßner,^[b] Armin Wedel,^{*, [b]} and Andreas Taubert^{*, [a]}



Metal sulfides are among the most promising materials for a wide variety of technologically relevant applications ranging from energy to environment and beyond. Incidentally, ionic liquids (ILs) have been among the top research subjects for the same applications and also for inorganic materials synthesis. As a result, the exploitation of the peculiar properties of ILs for metal sulfide synthesis could provide attractive new avenues for the generation of new, highly specific metal sulfides for numerous applications. This article therefore describes current

developments in metal sulfide nanoparticle synthesis as exemplified by a number of highlight examples. Moreover, the article demonstrates how ILs have been used in metal sulfide synthesis and discusses the benefits of using ILs over more traditional approaches. Finally, the article demonstrates some technological challenges and how ILs could be used to further advance the production and specific property engineering of metal sulfide nanomaterials, again based on a number of selected examples.

1. Introduction

Transition metal sulfide (TMS) nano- and microparticles have gained tremendous attention due to their interesting electrical, optical, chemical, catalytic, or mechanical properties.^[1,2] One of the most appealing aspects of metal sulfide nanoparticles is their diverse chemical compositions, particle morphologies, size, shape, and properties. As a result, changes in the chemical composition via doping, via the formation of solid solutions, or via the combination of multiple metals in a sulfide nanoparticle will provide access to a tremendous number of different types of nanoparticles with very specific (electro)chemical and physical properties.^[3] For example, metal sulfide nanoparticles have been studied for use in batteries, catalysts, light emitting diodes, solar cells, and many other fields.

Solar cells are among the most promising devices for solar energy conversion but challenges remain.^[4] For example, the current commercial silicon-based solar cell has disadvantages such as high cost, low energy efficiency, and lack of flexibility due to the rigid and thick wafer.^[5] As a result, thin-film solar cells (TSCs) have gained increasing interest as a replacement technology for conventional silicon solar cells. Due to their excellent optical and electrical properties, metal sulfide nanoparticles have been explored as functional components in various TSC types such as perovskite, copper indium sulfide (CIS), copper indium gallium sulfide (CIGS), copper indium gallium disulfoselenide (CIGSSe), organic, or dye sensitized solar cells (DSSC).^[6–15]

In this context, metal sulfide nanoparticles are predominantly explored for their potential as absorbers or charge (hole or electron) transport layers. Advantages of such an approach include (1) low cost, (2) light weight, (3) high flexibility in the design of the chemical and physical properties, (4) improved chemical and photochemical stability of the particles used in solar cell construction, and (5) good scalability via roll-to-roll processes compatibility with flexible materials.^[16,17] Consequently, numerous studies have addressed the fabrication of solar cells using metal sulfide nanoparticles as functional components with enhanced performance.

For example, Dowland et al. have fabricated CdS nanoparticle/polymer films using controlled thermal decomposition of a single-source metal xanthate precursor complex in solid-state poly(3-hexylthiophen-2,5-diyl), P3HT, polymer films as an active layer in heterojunction organic photovoltaic (OPV) cells.^[18] The resulting hybrid CdS/P3HT (5:1 wt%) film with a thickness of 100 nm annealed at 160 °C leads to an enhanced power conversion efficiency (PCE) from 1.45% to 2.17% with improved short circuit current (J_{sc}) of 4.848 mAcm⁻², open circuit voltage (V_{oc}) of 0.842 V and fill factor (FF) of 66%. This is attributed to the temperature-dependent nanomorphology of the CdS/P3HT film. Annealing at 160 °C results in CdS/P3HT hybrid active layers with small domains with sizes below 40 nm. This produces a higher charge photogeneration yield.


Yang et al. successfully generated CdS and Sb₂S₃ nanocrystals inside P3HT/PC₆₁BM (phenyl-C₆₁-butyric acid methyl ester) hybrids via simply mixing cadmium or antimony xanthate precursors and a polymer solution and a subsequent annealing step at 160 °C for 30 min.^[19] The resulting 3 wt% CdS nanoparticles embedded in the polymer film provide improved optical absorption, improved hole mobility, and improved surface roughness compared to the pristine polymer absorbing layer. The addition of CdS or Sb₂S₃ nanoparticle improves J_{sc} of the device due to the high hole mobility of the two TMSs of 1.53 × 10⁻⁴ cm²V⁻¹s⁻¹ and 1.69 × 10⁻⁴ cm²V⁻¹s, respectively. Higher hole mobilities reduce the carrier imbalance in the active layer and therefore they improve J_{sc} , FF, and thus the PCE to 2.91% and 2.92%.


Bi et al. showed that NiS and CoS nanoparticle-coated graphene layers are suitable DSSC counter electrodes.^[20] The authors made NiS and CoS nanoparticles directly on graphene films by thermal decomposition of nickel ethyl xanthate Ni(C₃H₅OS₂)₂ and cobalt ethyl xanthate Co(C₃H₅OS₂)₂. This process results in 5–20 nm hexagonal NiS and cubic Co₉S₈ nanoparticles with high electrocatalytic activity and cell

[a] C. Balischeckski,⁺ K. Behrens, A. Beqiraj, T. Körzdörfer, Prof. Dr. A. Taubert
Institute of Chemistry
University of Potsdam
Karl-Liebknecht-Str. 24–25
14476 Potsdam (Germany)
E-mail: ataubert@uni-potsdam.de

[b] H.-S. Choi,⁺ A. Geßner, Dr. A. Wedel
Fraunhofer Institute for Applied Polymer Research (IAP)
Functional Materials and Devices/Functional Polymer Systems
Geiselbergstrasse 69
14476 Potsdam-Golm (Germany)
E-mail: armin.wedel@iap.fraunhofer.de

[⁺] These authors contributed equally to the work.

 An invited contribution to a Special Issue dedicated to Material Synthesis in Ionic Liquids

 © 2021 The Authors. Published by Wiley-VCH GmbH. This is an open access article under the terms of the Creative Commons Attribution Non-Commercial License, which permits use, distribution and reproduction in any medium, provided the original work is properly cited and is not used for commercial purposes.

efficiencies of 5.25% (NiS) and 5.04% (Co_9S_8), respectively, compared to 5.00% of the pure graphene film with a conventional Pt electrode. The main advantage here is not necessarily the fact that the efficiency is somewhat higher but also that the rather expensive Pt catalyst can be replaced by much cheaper alternatives.

In the same vein, semiconductor nanoparticle-sensitized solar cells (NSSCs), which are conceptually derived from DSSCs, are low-cost alternatives to conventional photovoltaic devices. Similar to the study just described, Boon-on et al. successfully introduced ternary $\text{Pb}_x\text{Cd}_{1-x}\text{S}$ nanoparticles into the counter electrode of NSSCs via a two-stage sequential ionic layer adsorption reaction (SILAR) method.^[21] The band gap of the metal sulfide nanoparticles was tuned by the Pb contents to improve the light-absorbing window from 500 to 720 nm, producing cells with efficiencies of 8.48%, V_{oc} of 0.60 V, J_{sc} of 0.19, and an FF of 73.5%.

As metal sulfides often have high hole concentrations, sulfides like nickel sulfide (NiS) and copper sulfide (CuS) are often exploited as p-type hole transport layers in organic solar cells or as dopants in perovskite solar cells to overcome the poor charge transport in the polymer layer.^[22] Hamed et al. incorporated NiS nanoparticles into conventional carbon paste and this nickel-carbon composite hole transport layer resulted in an improved conversion efficiency compared to a pure NiS electrode from 1.87% to 5.20%.^[23] The authors assigned this improvement to the existence of local surface plasmon resonance absorption and light scattering processes.

Moreover, metal sulfides have also been studied as electron transport layers (ETLs) in perovskite solar cells due to their availability, suitable energy-level and room temperature processability. However, these approaches use evaporated thin films rather than nanoparticles.^[8]

Besides solar cells, electroluminescent-quantum dot light emitting diodes (EL-QLED) are another interesting field of application for metal sulfide nanoparticles.^[24] EL-QLEDs are explored as technology platforms for next generation displays.

They are expected to overcome the disadvantages of conventional organic light emitting diodes (OLED), such as burn-in phenomena, short lifetime, high cost, and complexity of materials development.^[25]

The most common component in EL-QLED devices consisting of metal sulfides is the emissive layer. Chalcopyrite CuInS_2 nanoparticles are representative emissive materials with low band gap of 1.5–2.0 eV with high quantum yield, broad color tuneability, and wide absorption window. Moreover, CuInS_2 has the added advantage that it contains no toxic Cd and Pb. For example, Kim et al. reported high efficiency CuInS_2 EL-QLEDs with over 7% of external quantum efficiency and outstanding current efficiency of 18.2 cd/A .^[26]

Similarly, PbS nanoparticles are characterized by their long emission wavelength of over 1100 nm which renders them suitable for infrared (IR) EL-QLED, IR sensors, bioimaging, and other long wavelength applications. Marus et al. reported bright and stable halide-capped PbS-based EL-QLED in combination with a thin aluminum oxide layer, which can suppress the electron mobility to adjust the charge balance in the active layer.^[24] This resulted in $7 \text{ Wsr}^{-1} \text{ m}^{-2}$ peak radiance at 1.3 μm wavelength.

Besides applications exploiting the optical or electronic properties of metal sulfide nanoparticles, the electrochemical and chemical properties of these materials have also attracted attention. Two major fields have been explored: applications in (electro)catalysis and batteries. Among others, bimetallic sulfides (BMSs) with high (theoretical) capacity and outstanding redox reversibility has shown great promise as high-performance anode materials for conventional lithium-ion batteries (LIB) and next-generation energy storage systems, such as sodium ion batteries (SIB) and sodium magnesium ion batteries (SMI).^[1,27,28]

Specifically, due to the effective lithium storage in metal sulfides through reversible Li_2S conversion and Li-metal alloying, metal sulfide anodes can outperform the current electrode materials in LIB with two or three times higher capacities.^[29,30]



Armin Wedel studied Physics at the University of Rostock and obtained his doctorate in Physics from the University of Potsdam in 1992 while working at the Institute of Polymer Chemistry of the Academy of Science in Teltow. In 1992 he joined the FhI-IAP, where he is now the Division Director of Functional Polymers. His research interests are light emitting materials, solar energy conversion materials, and environmentally friendly quantum dots. He holds over 18 patents, has published over 70 publications, and is a recipient of the Award of the Korean Information Display Society. He is the President of the German Flat Panel Forum (DFF e.V.) and a member of the overseas advisory boards of the International Conference on Display Technology (ICDT, China) and the International Meeting on Information Displays (IMID, Korea).



Andreas Taubert is a professor of Supramolecular Chemistry and Materials Chemistry at the University of Potsdam. Previous stations include the University of Basel, the Max Planck Institute for Polymer Research, the University of Michigan, the University of Pennsylvania, and the Max Planck Institute of Colloids and Interfaces. Originally starting in bioinspired materials synthesis, his current research interests include materials chemistry in and with ionic liquids, inorganic and hybrid energy materials, and materials for water remediation. Andreas Taubert is an international member of the African Center for Excellence in Water and Environmental Research in Nigeria and has held a number of fellowships and visiting professorships worldwide. Besides chemistry and materials, he likes to spend time on his trumpet, flugelhorn, and bass trumpet.

However, the large volume expansion of metal sulfide during lithium conversion leads to poor electrochemical properties of lithium-ion batteries.^[31] This problem has been addressed by combining metal sulfides with carbon materials, such as graphene, carbon nanotubes (CNTs), and spherical carbon producing materials with high conductivity, flexibility, large surface area, and chemical stability.^[32–34]

Zhang et al. successfully grew ZnS nanoparticles on the surface of CNTs supported by the defect site on the CNTs as effective reaction active sites. ZnS–CNTs exhibit fast electron transfer caused by the conductive CNT network, as well as enhanced electrochemical reaction, and quick ion transport from homogeneously distributed ZnS nanoparticle.^[3] This composite structure achieves good rate performance and excellent cyclability at high current density (reversible capacity of 451.3 mAh g⁻¹ after 1200 cycles at 5 Ag⁻¹, 377.8 mAh g⁻¹ at 8 Ag⁻¹).

Besides anodes, metal sulfides have also been studied in cathodes, for example in alkali metal-sulfur batteries.^[1,35,36] This is not a recent development, but metal sulfide-based cathodes have attracted increasing attention in the recent past.^[37,38] For example, Xiao et al. have reported a general approach towards various metal sulfides with a wide range of morphologies.^[39] The major advance in this study is a proof-of-concept experiment showing that CuS deposited on a Cu foil acts as a binder-free cathode with an initial reversible capacity of 588 mAh g⁻¹ at 56 mA g⁻¹ with a rather small capacity fading rate of 0.17% per cycle over the course of 100 cycles. Moreover, this material exhibits a good high-rate capability of up to 463 mAh g⁻¹ at 2.8 Ag⁻¹.

Among others, metal sulfide/carbon composites have been studied for their performance in cathodes.^[40] For example, He et al. demonstrated that the combination of a rather open carbon support (“carbon sponge”) with metal sulfide nanodots leads to an increased performance largely by successful suppression of the Li-polysulfide shuttle effect. Similarly, Nazar and coworkers demonstrated that metallic Co₉S₈ with an interconnected sheet-like morphology resembling graphene is an efficient material to control dissolution and precipitation in an electrochemical cell and therefore leads to highly improved performance in Li–S batteries.^[41] Overall, these few examples clearly show that the high compositional and structural variability makes metal sulfide interesting candidates for both cathode and anode materials.

Furthermore, transition metal sulfides have gained significant attention as electrode material for electrochemical supercapacitor (ESs) because of their good electrical conductivity and high specific capacity.^[229] ESs have been investigated as future flexible energy storage devices due to their high-power density, fast charging, and good cyclability and TMSs have been identified as a key component for their high performance.^[230–231] For instance, Liu et al. made ternary Co_{0.33}Fe_{0.67}S₂ nanoparticles by sulfidation on graphene nanosheets. The resulting materials exhibit superior electrochemical characteristics with nearly complete capacitance retention of 102.2% even after 10,000 cycles.^[229] The electrochemical activation of the electrode surface after the sulfidation leads to an improved capacitance

retention which the authors have assigned to the improved wettability of electrode material.

Finally, metal sulfides are effective catalysts for a series of chemical reactions including industrial processes.^[42–45] Recent examples include electrocatalytic ammonia formation or water splitting.^[46,47] For example, Girault and coworkers showed that ternary molybdenum sulfides MMoS_x (M = Fe, Co, Ni, Mn) are attractive alternatives to noble metal catalysts for hydrogen formation using a heterogeneous system at the polarized water/dichloromethane interface using decamethylferrocene.^[48] Also using a composite sulfide approach, Hong et al. have shown that the combination of various transition metal sulfides can provide effective catalysts for photochemical hydrogen evolution.^[49] In a particularly elegant example, Kudo and coworkers have shown that a Z-type architecture involving a variety of p-type semiconductor metal sulfides can lead to effective catalysts for H₂ evolution.^[50] Finally, Chen et al. demonstrated the synthesis and application of a porous Ni₃S₂-based electrode for both the hydrogen (HER) and the oxygen evolution reaction (OER).^[51]

Considering all of the above and beyond, it is clear that metal sulfides are a highly interesting class of materials with a tremendous application potential (Figure 1). In spite of their broad diversity and the high number of synthesis protocols that are available, metal sulfides are far from being perfect and a number of challenges remain: for example, (1) suitable synthesis protocols are not always available, (2) scalability of the synthesis may be an issue, (3) some synthetic protocols use high temperatures which often lead to thermodynamic rather than kinetic products, and (4) nonstoichiometric compositions are not always easily accessible. As a result, scalable low temperature syntheses able to also produce unstable or metastable metal sulfide nanoparticles are still highly sought after. Ideally, these processes should also be low(er) cost and environmentally friendly.

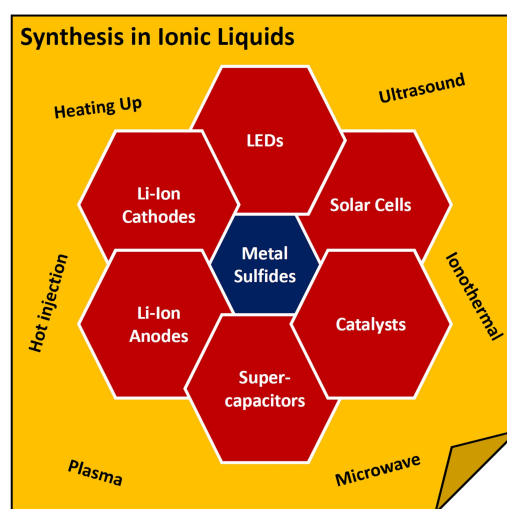


Figure 1. General overview of synthetic methods and selected applications of TMSs. Other applications include environmental materials, photo- and electrocatalysts.

One approach that may provide some of these possibilities is the synthesis of metal sulfides in and from ionic liquids (ILs). ILs provide an interesting and highly flexible synthesis environment for inorganic (materials) synthesis and therefore ILs have been explored for nanoparticle synthesis as well. Some of the key advantages are (1) their high solubilizing power for many salts and organic compounds, (2) their often high thermal and electrochemical stability, (3) their very low vapor pressure, and (4) their very high structural and chemical variability, which provides access to a wide range of IL properties. Moreover, as they are ionic in nature, they provide an ideal reaction medium for the synthesis of materials based on charged building blocks such as metal cations.^[52–56]

The current article therefore highlights some approaches using ILs for the synthesis of metal sulfides. In particular, we show that there are different approaches, different groups of compounds, and interesting materials properties that can be generated by using a suitable combination of precursor, IL, and reaction condition to produce a wide variety of often highly interesting sulfides with high application potential.

2. Metal Sulfide Nanoparticle Synthesis Without ILs

Before discussing the synthesis involving ILs it is worthwhile to briefly reflect on existing metal sulfide synthesis approaches that do not use ILs. This will help to better understand and distinguish the effects that are generally known from metal sulfide synthesis from those that are rather unique or at least prominent to IL-based synthesis approaches.

One of the important early advances that was widely publicized in the 1990s is the concept of controlled single jet and double jet precipitation (CSJP and CDJP, respectively).^[57] In this approach, using a syringe pump, solutions containing precursors are added to a large volume of liquid typically containing a second component. Upon addition of the precursor solutions to the liquid volume, the two reaction partners can react and form nano- or microparticles. The approach has two interesting aspects: (1) the concentration of precursors is very high at the addition point and thus this is the only location in the reaction volume where nucleation occurs. Additionally (2) the reaction conditions can be adjusted by varying the concentrations of the precursor solution, the solvents, and in particular, the addition rate. As a result, there are numerous studies exploiting the use of these techniques for the controlled synthesis of (among others) various metal sulfide particles, most of them in the micrometer size range.^[58,59]

Later on, the quest for smaller particles led to the development of various other approaches such as methods involving temperature ramps (heating up methods) or the hot injection approaches.^[60,61] Generally, hot injection exploits the fact that hot solutions containing the metal precursor are an efficient reaction medium to very rapidly nucleate nanoparticles. This is largely due to the fact that the reaction temperatures lead to a rapid sulfur (i.e. H₂S) release from the injected sulfur sources

and hence a rapid and very uniform crystal nucleation and growth is typically observed.^[62–66]

In contrast, temperature ramp methods involve the preparation of a suitable precursor solution at room temperature, subsequent heating (often exploiting specific temperature profiles), and a cooling step. These reactions are based on the use of sulfur sources that are stable at room temperature but decompose at higher temperatures and again form the metal sulfide via intermediate H₂S formation, similar to the hot injection approaches just described. In fact, the sulfur sources used in the heating up syntheses are often quite similar, such as alkyl thiols, ammonium sulfide, carbamates, or elemental sulfur.^[63,67–71] Other examples also include cysteine, which is interesting from a sustainability viewpoint.^[72] Figure 2 illustrates some examples of metal sulfides made using a variety of sulfur sources.

Hydrothermal and solvothermal reactions have also attracted interest for metal sulfide synthesis. To a large extent this is inspired by the fact that hydrothermal vents produce a large variety of metal sulfides.^[73] For example, Ikkurthi et al. have shown that hydrothermal reactions are effective for the production of CoS, CuS, FeS, and NiS powders for supercapacitor electrodes.^[74] Similarly, Bolagam and Um have used a related approach to produce Co₂RuS₆ for application in pseudocapacitors.^[75] Ermadi et al. used a variety of (renewable) sulfur sources to synthesize a wide range of (transition) metal sulfides.^[76] In a very interesting study, Pring and coworkers demonstrated that quite complex metal sulfides can be synthesized via hydrothermal reactions. The main advantage as pointed out by the authors is the fact that their approach of hydrothermal dissolution-precipitation is highly suitable for the synthesis of thermally less stable materials,^[77] (Figure 3). Furthermore, Moore et al. showed that greigite nanoparticles can be synthesized via hydrothermal reaction and that only the hydrothermal reaction yielded the desired greigite products. A

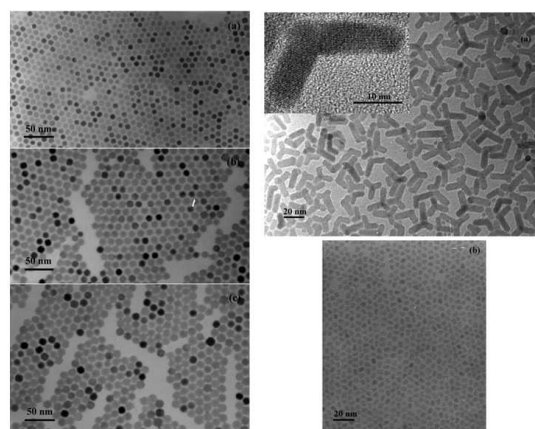


Figure 2. Left: TEM images of (a, top) 6 nm, (b, middle) 8 nm, and (c, bottom) 9 nm sized PbS nanocrystals. Right: TEM images of CdS nanocrystals. (a) Mixture of rods, bipods, and tripods with an average size of 5.4 nm (thickness) × 20 nm (length); inset is a HRTEM image of a single CdS bipod-shaped nanocrystal. (b) Spherical nanoparticles with an average diameter of 5.1 nm. Reprinted with Permission from Joo et al., *Journal of the American Chemical Society* **2003** 125 (36), 11100–11105.^[71] Copyright 2020 American Chemical Society.

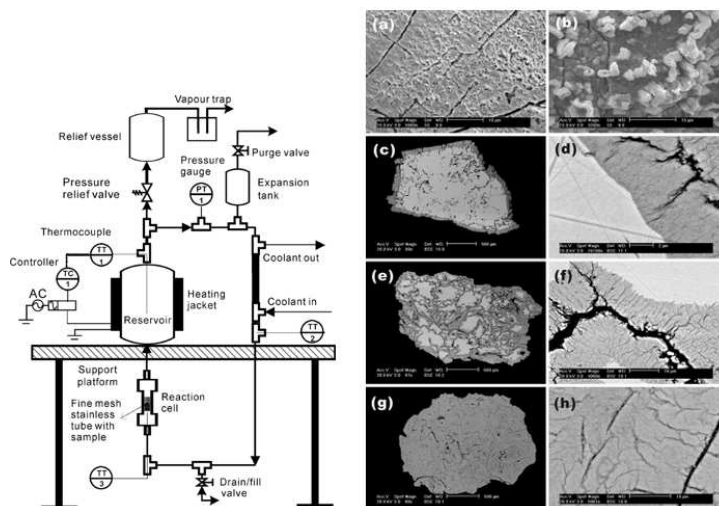


Figure 3. Schematic representation of the hydrothermal synthesis setup and images of materials obtained from these reactions. The electron images show the samples as they form under different conditions vs. reaction time. Left: Schematic diagram of the 316 stainless steel therosyphon driven flow-through hydrothermal cell. The volume of the reservoir, the expansion tank, and the cell are 150, 75, and 25 mL, respectively. The total internal volume of the cell, including tubing, is 260 mL. Right: selected SEM micrographs and backscattered electron images of samples using various precursors at different reaction times. Reprinted with Permission from Xia et al., *Chemistry of Materials* 2008 20 (8), 2809–2817.^[77] Copyright 2020 American Chemical Society.

standard precipitation route failed.^[78] This clearly shows that hydrothermal reactions are useful in shifting the outcome to products that cannot be accessed otherwise or at least not as easily.

Finally, microwave and ultrasound synthesis of metal sulfide nanoparticles has been described. Both approaches have attracted interest because they can introduce rather high amounts of energy into a reaction vessel in very short times. Often, this produces very homogeneous reaction conditions throughout the reaction vessel yielding uniform products.^[79,80] For example, Cao and coworkers have shown that microwave reactions can provide access to metal sulfides such as CoS_x with application potential as electrocatalysts for water splitting,^[81] (Figure 4). Among others, copper sulfide nanomaterials have also been shown to exhibit plasmonic coupling, a feature that could be interesting for non-noble metal based plasmonics.^[82] Such approaches and materials have been studied for a number of different applications, such as Li ion batteries, supercapaci-

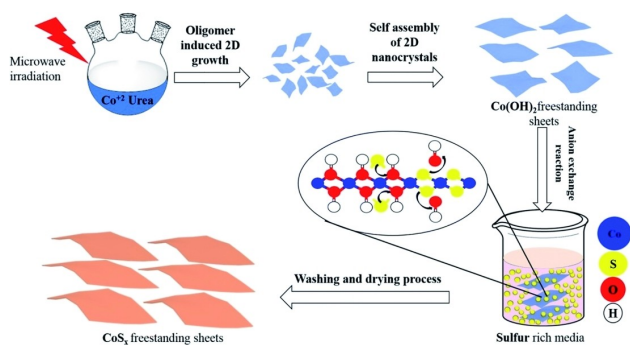


Figure 4. Schematic of the preparation process of CoS_x freestanding sheets. Reproduced from Souleyman et al., *J. Mater. Chem. A*, 2018, 6, 7592–7907,^[81] with permission from The Royal Society of Chemistry 2020.

tors, photocatalysts, or materials for solar cells. Similar reports exist for ultrasound assisted reactions.^[39,83–88]

A further development that goes along with these methodological approaches is the use of a wide variety of precursors. Many approaches involve simple metal salts and a wide variety of sulfur sources, most of which decompose at higher temperatures to produce the final metal sulfides.^[62–72,82]

A particularly interesting approach, however, is the use of single source precursors, where a precursor molecule contains both the sulfur atom(s) and all metal ions required for the formation of the final product,^[89–93] (Figure 5). Examples of such single source precursors include xanthates, dithiocarbamates, thiooxalates, and others.^[62,82,94–104]

The specific appeal of single source precursors is not only that all components of the products can be present in one single compound but also that the stoichiometry can directly be pre-programmed and as such allows for a quite straightforward tuning of the composition (and hence the physical properties) of the final product. This is particularly interesting if unusual or otherwise challenging structures and compositions are desired.

A further possibility for metal sulfide synthesis is the use of mechanosynthetic approaches but as the major focus of this article is on liquid phase synthesis, this will not be discussed here.^[106–109] Excellent recent reviews on the subject can be found in refs.^[110,111]

3. Metal Sulfide Nanoparticle Synthesis with ILs

Over the last decades, Ionic Liquids (ILs) have gathered a lot of interest as a research field. Traditionally, ILs are salts with melting points below ca. 100 °C, although this boundary is rather arbitrary. ILs have been explored for the synthesis of

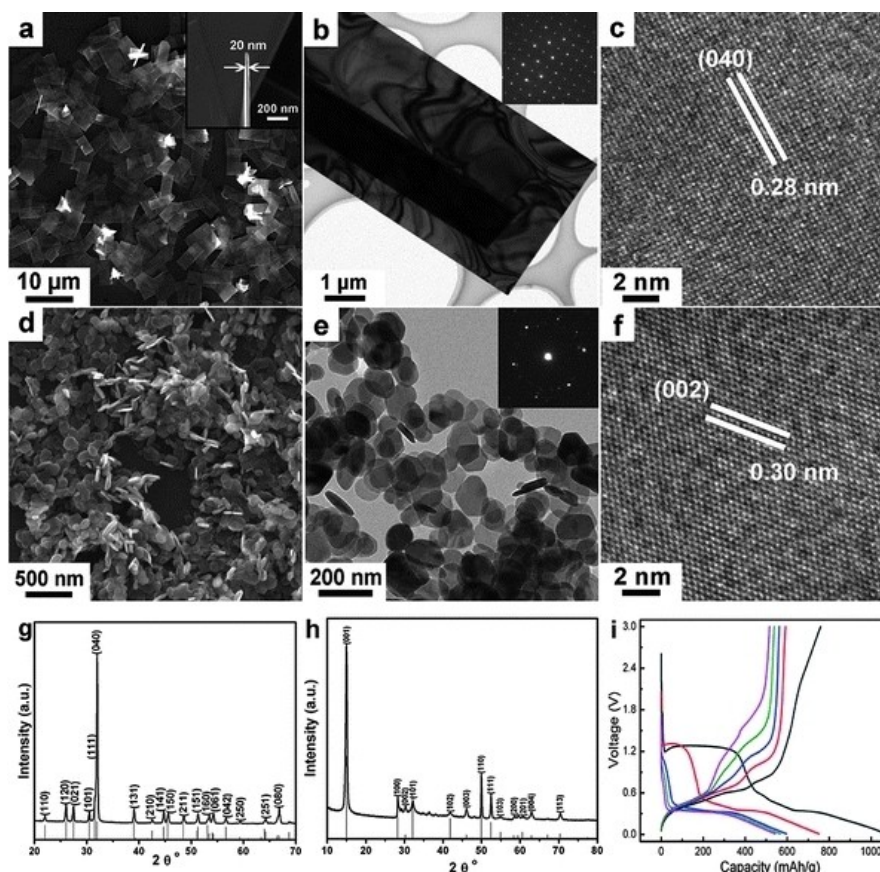


Figure 5. SEM, TEM and HRTEM images of SnS nanosheets (a–c) and SnS₂ nanoplates (d–f). XRD patterns of SnS nanosheets (g) and SnS₂ nanoplates (h). (i) Discharge-charge profiles for the SnS nanosheets under a current of 50 mA g⁻¹ and voltage range of 3.0–0.01 V. Reproduced from Shen et al., *CrystEngComm*, 2011, 13, 4572–4579,^[89] with permission from The Royal Society of Chemistry 2020. Original data published in Zhang et al., *Chem. Commun.*, 2011, 47, 5226–5228,^[105] Reproduced from Zhang et al., *Chem. Commun.*, 2011, 47, 5226–5228,^[105] with permission from The Royal Society of Chemistry 2020.

chalcogenides acting as a reaction medium or as a starting material.^[112–115] Hereby, metal-containing ionic liquids (MILs) are a particularly interesting class of starting materials for the IL-assisted metal chalcogenide synthesis. Some of these MILs have been termed ionic liquid precursors (ILPs)^[116,117] because they can act as a solvent, a metal precursor, and a template for particle formation at the same time (although no *single source* precursor ILPs have been reported so far – the sulfur always needs to be added separately to the reaction).^[52,118–131] Consequently, MILs have gathered a lot of attention as “all-in-one solvent-template-reactants”.^[123]

ILs show interesting and unusual properties, such as high thermal and chemical stability, non-flammability, electronic and ionic conductivity, negligible vapor pressure, and a broad electrochemical stability window.^[124,128,132–134] Furthermore, ILs are highly effective solvents for both organic and inorganic compounds and can also be used in high vacuum environments.^[135,136] Additionally, the use of ILs is also applicable to environments where water and other polar solvents cannot be used.^[137–139]

Another advantage of ILs is the high flexibility in their chemical composition. As a result, specific chemical, physical, or biological properties of ILs can be tailored by changing the

anionic or cationic part of the IL or by altering specific functional groups.^[128,133] This unique possibility to adjust chemical, physical, and biological properties over a very wide range has led to ILs being used in virtually infinite numbers of applications such as electrolytes in batteries, photovoltaic cells, fuel cells, and actuators.^[140–144] Due to their many advantages and beneficial properties, ILs have also been used in a multitude of different synthetic approaches, including materials and particle synthesis.

Some work has also been dedicated to exploring the potential of ILs for the synthesis of metal sulfide (nano) materials. The following paragraphs will describe and discuss these approaches and attempt at providing an overview over the concepts, successes, and open questions in the general field of metal sulfide synthesis using ILs. While the focus is on synthetic approaches, the characteristics of the products and the application potential of some materials will also be highlighted. Table 1 summarizes these studies and the text below will provide further details.

Very similar to reactions in molecular liquids, hot injection reactions are among the most common synthetic approaches for metal sulfide synthesis. Usually, the sulfur source is added to a preheated solution, which contains the metal precursor.

Table 1. Overview over synthetic approaches towards metal sulfides using ILs. SSP is single source precursor, NP stands for nanoparticles, NC is nanocrystals, E_g stands for the energy of the direct optical band gap, THTDP is trihexyl(tetradecyl)phosphonium, EMI stands for 1-ethyl-3-methylimidazolium, BMIm is 1-butyl-3-methylimidazolium, TAA is thioacetamide, ChCl stands for choline chloride, OLAHS is oleylammonium hydrosulfide, and MSTL stands for mesitylene.

Exp. Approach	Metal source	IL	Sulfur Source	Exp. Parameters	Morphology	Crystal Structure	E_g	Ref
Hot Injection	$\text{Cu}[\text{S}_2\text{CN}(\text{C}_2\text{H}_5)_2]_2$ [SSP]	(THTDP)N(CN) ₂	$\text{Cu}[\text{S}_2\text{CN}(\text{C}_2\text{H}_5)_2]_2$ [SSP]	3 h, 120/180/240 °C	Cubic (43 nm, 120 °C), rhombohedral (30 nm, 180 °C), monoclinic (22 nm, 240 °C) NC,	$\text{Cu}_{1.8}\text{S}$ (digenite) at 120–180 °C, $\text{C}_{1.94}\text{S}$ at 240 °C	CuS 2.2 eV, $\text{C}_{1.94}\text{S}$ 1.4 eV, $\text{C}_{1.8}\text{S}$ 1.75 eV	[112]
	$\text{Cu}[\text{S}_2\text{CN}(\text{C}_4\text{H}_9)_2]_2$ [SSP]	(THTDP)NTf ₂	$\text{Cu}[\text{S}_2\text{CN}(\text{C}_4\text{H}_9)_2]_2$ [SSP]	3 h, 120/180/240 °C	Monoclinic (11 nm, 180 °C), rhombohedral (42 nm, 240 °C) NC	$\text{Cu}_{1.94}\text{S}$ (djurleite) at 180 °C, $\text{C}_{1.8}\text{S}$ at 240 °C		
	$(\text{C}_{12}\text{Py})_2[\text{CuCl}_4]$	$(\text{C}_{12}\text{Py})_2[\text{CuCl}_4]$	(TMS) ₂ S	4 h, 120 °C	hexagonal plates NP, 30–680 nm	CuS (covellite)	2.3 eV	[113]
	$\text{Pb}(\text{OAc})_2 \times 3\text{H}_2\text{O}$	(EMIm)(CH ₃ SO ₃)	Dodecanthiol	1 h, 200/250 °C	200 °C: cubic/hexagonal NP 45–86 nm; 250 °C: 45–86 nm	–	–	[145]
	$\text{Pb}(\text{OAc})_2 \times 3\text{H}_2\text{O}$	(EMIm)(CH ₃ SO ₃)	Na ₂ S	30 min, 150/200 °C	150 °C: rectangular/spherical, 38 nm; 200 °C: branched/spherical, 37 nm	–	–	
Heating Up	$\text{Pb}(\text{S}_2\text{COCH}_2\text{CH}_3)_2$ [SSP]	(EMIm)(CH ₃ SO ₃)	$\text{Pb}(\text{S}_2\text{COCH}_2\text{CH}_3)_2$ [SSP]	30 min, 150/200 °C	150 °C: cubic NP, 64–102 nm; 200 °C: cubic/spherical NP, 55–160 nm)	–	–	
	$\text{Pb}(\text{OAc})_2 \times 3\text{H}_2\text{O}$	(BMIm)BF ₄	TAA	15 min, 100 °C	cubic NP 10 nm	cubic space group <i>Fm3m</i>	–	[146]
	$\text{Cu}[\text{S}_2\text{CN}(\text{C}_2\text{H}_5)_2]_2$ [SSP]	(THTDP)N(CN) ₂	$\text{Cu}[\text{S}_2\text{CN}(\text{C}_2\text{H}_5)_2]_2$ [SSP]	3 h, 180 °C	cubic(120 °C)/rhombohedral(180 °C)/monoclinic (240 °C) NC, 43–30–22 nm	$\text{Cu}_{1.8}\text{S}$ (digenite) at 120–180 °C, $\text{C}_{1.94}\text{S}$ at 240 °C	CuS 2.2 eV, $\text{C}_{1.94}\text{S}$ 1.4 eV, $\text{C}_{1.8}\text{S}$ 1.75 eV	[112]
Solid state	$\text{Cu}[\text{S}_2\text{CN}(\text{C}_4\text{H}_9)_2]_2$ [SSP]	(THTDP)NTf ₂	$\text{Cu}[\text{S}_2\text{CN}(\text{C}_4\text{H}_9)_2]_2$ [SSP]	3 h, 180 °C	monoclinic(180 °C)/rhombohedral (240 °C) NC, 11–42 nm	$\text{Cu}_{1.94}\text{S}$ (djurleite) at 180 °C, $\text{C}_{1.8}\text{S}$ at 240 °C		
	ZnCl ₂	–	CaS/Na ₂ S	Steel ball mill, Aratm.	Cubic NP, 8–16 nm	ZnS (zinc blende/sphalerite)	–	[106]
	CdCl ₂	–	CaS/Na ₂ S	Steel ball mill, Aratm.	Hexagonal/ cubic NP, 4–8 nm	CdS (wurtzite/sphalerite structure)	–	
	CeCl ₃	–	CaS/Na ₂ S	Steel ball mill, Aratm.	Tetragonal/ cubic NP, 20–32 nm	$\beta\text{-Ce}_2\text{S}_3$, $\gamma\text{-Ce}_2\text{S}_3$	–	
	Zn(OAc) ₂	–	Na ₂ S	Steel ball mill, 350 rpm, 2–10 h, Aratm.	Hexagonal NP, 2–5 nm	ZnS (sphalerite/wurtzite)	3.87 eV	[107]
	Pb(OAc) ₂	–	Na ₂ S	Steel ball mill, 350 rpm, 2–10 h, Aratm.	Cubic NP, 8–25 nm	PbS (galena)	3.54 eV	
	Cd(OAc) ₂	–	Na ₂ S	Steel ball mill, 350 rpm, 2–10 h, Aratm.	Cubic/ hexagonal NP, 8–13 nm	CdS (hawleyite/greenockite)	3.65 eV	
	Cu(OAc) ₂	–	Na ₂ S	Steel ball mill, 350 rpm, 2–10 h, Aratm.	Shapeless NP, 6–8 nm	CuS (covellite), CuSO ₄ (bonattite)	3.54 eV	
Ultrasound	ZnCl ₂	–	CaS	Steel ball mill, 2–36 h, Aratm.	Shapeless NP, 6–30 nm	ZnS (sphalerite)	–	[147]
	$\text{Zn}(\text{OAc})_2 \times 2\text{H}_2\text{O}$	(C _x MI)NTf ₂ (x = 4–8)	TAA	60 min, 15 °C, 20 kHz	cubic NP (12 nm)	–	4.86–5.77 eV	[148]
	SnCl ₂	(BMIm)BF ₄	TAA	10 min, RT, 20 kHz	polygonal NP, Grape-like NP, Potato-like NP; 350–450 nm	Orthorhombic SnS	1.7–2.3 eV	[115]
Cd(OAc) ₂	(EMIm)(EtSO ₄)	TAA	60 min, RT, 23 kHz	IL + H ₂ O: (nearly) spherical (150–300 nm); IL: 50–100 nm, all agglo.	–	2.42 eV	[149]	

Table 1. continued								
Exp. Approach	Metal source	IL	Sulfur Source	Exp. Parameters	Morphology	Crystal Structure	E_g	Ref
Microwave	Bi_2O_3	(BMIm)BF ₄	$\text{Na}_2\text{S}_2\text{O}_3$	30s/10 min, 190 °C	nanorods (30s: < 80 nm; 10 min: < 60 nm)	–	–	[150]
	Sb_2O_3	(BMIm)BF ₄	$\text{Na}_2\text{S}_2\text{O}_3$	40 min, 165 °C	nanorods (length 3 μm , diameter 200 nm)	–	–	
	$\text{Zn}(\text{OAc})_2 \times 2\text{H}_2\text{O}$	(BMIm)BF ₄	$\text{Na}_2\text{S} \times 9\text{H}_2\text{O}$	10 min, 100 °C	spherical NP (3.5 nm)	–	–	[151]
	$\text{CdCl}_2 \times 2.5\text{H}_2\text{O}$	(BMIm)BF ₄	$\text{Na}_2\text{S} \times 9\text{H}_2\text{O}$	10 min, 100 °C	spherical NP (7 nm)	–	–	
	$\text{Zn}(\text{OAc})_2 \times 2\text{H}_2\text{O}$	(EMIm)(EtSO ₄)	TAA	4 min, RT	spherical NP (1:1 H ₂ O/IL: 200–600 nm; 1:4 H ₂ O/IL: smaller)	–	–	[152]
	$\text{Zn}(\text{OAc})_2$	(C ₄ MIm)NTf ₂	TAA	60 min, 15 °C	cubic NP (6 nm)	–	4.86–5.77 eV	[148]
Ionothermal (autoclave)	$\text{Pb}(\text{OAc})_2 \times 3\text{H}_2\text{O}$	ChCl	TAA/ChCl	15 h, 150/180 °C	Octahedrally shaped crystals (300 nm)	cubicPbS (galena)	–	[153]
	$\text{Cd}(\text{OAc})_2 \times 2\text{H}_2\text{O}$	ChCl	TAA/ChCl	15 h, 150/180 °C	spherical NP (30 nm)	greenockite, hexagonal space group <i>P63mc</i>	–	
	AgNO_3	ChCl	TAA/ChCl	15 h, 150/180 °C	polyhedral (2–8 μm)	monoclinic Ag ₂ S (acanthite, <i>P21/n</i>)	–	
	$\text{Zn}(\text{NO}_3)_2 \times 6\text{H}_2\text{O}$	ChCl	TAA/ChCl	15 h, 150/180 °C	platelets (200 nm), microsphere (4.5 μm)	Zn blende (sphalerite), hexagonal wurtzite	–	
	$\text{Bi}(\text{NO}_3)_3 \times 5\text{H}_2\text{O}$	ChCl	TAA/ChCl	15 h, 150/180 °C	flowers composed of nanowires (30 nm)	orthorhombic Bi ₂ S ₃ (bismuthinite, <i>Pnma</i>)	–	
	$\text{Sb}(\text{OAc})_3$	ChCl	TAA/ChCl	15 h, 150/180 °C	stacked sheets (50 nm), after 350 °C: rods agglomerated to plates	orthorhombic Sb ₂ S ₃ (stibnite, <i>Pnma</i>)	–	
	$\text{Cu}(\text{NO}_3)_2 \times 3\text{H}_2\text{O}$	ChCl	TAA/ChCl	15 h, 150/180 °C	hexagonal plates (20–70 μm)	covellite CuS, hexagonal crystal (<i>P63Immc</i>)	–	
	$\text{CuCl}_2 \times 2\text{H}_2\text{O}$	(BMIm)BF ₄	S8, CS ₂	24 h, 130 °C	nestlike hollow spheres composed of flakelike microcrystals (5–8 μm)	covellite CuS, hexagonal crystal	–	[154]
	$\text{Zn}(\text{OAc})_2 \times 2\text{H}_2\text{O}$	(BMIm)BF ₄	TAA	5 h, 180 °C	Hexagonal planes NP 3 nm	hexagonal space group <i>P63mc</i>	–	[146]
	$\text{Cd}(\text{OAc})_2 \times 2\text{H}_2\text{O}$	(BMIm)(MeSO ₄)	TAA	5 h, 180 °C	hexagonal CdS NP (4 nm)	hexagonal space group <i>P63mc</i>	–	
		(BMIm)BF ₄	TAA	5 h, 180 °C	hexagonal CdS NP (7 nm)	hexagonal space group <i>P63mc</i>	–	
		(BMIm)BF ₄	TAA	5 h, 180 °C	hexagonal CdS Nanorods (7 nm)	hexagonal space group <i>P63mc</i>	–	
(BMIm)PF ₆		TAA	5 h, 180 °C	hexagonal CdS NP (13 nm)	hexagonal space group <i>P63mc</i>	–		
Precipitation	$\text{Cu}(\text{OAc})_2 \times \text{H}_2\text{O}$	(C ₄ C ₂ OOHIm)NTf ₂	Na ₂ S	RT, 15 min	plate-like nanostructures, self-assembled large plates	–	–	[155]
	$\text{Cu}(\text{OAc})_2 \times \text{H}_2\text{O}$	(C ₄ C ₂ OOHIm)NTf ₂	TAA	80 °C, 15 min	plate-like nanostructures, form rough spheroidic structures	–	–	
	AgNO_3	OLAHS	OLAHS in MSTL	60 min, RT	NP 8–9 nm	acanthite Ag ₂ S	–	[65]
	AgNO_3 , Au–NP/OLA	OLAHS	OLAHS, H ₂ S	10 min, 80 °C → RT, H ₂ S	Janus-particles (Au@Ag ₂ S), 8–9 nm	acanthite Ag ₂ S	–	
CuOAc	OLAHS	OLAHS in MSTL	80 °C, 20 min → 26 h RT	spherical NP, 4–7 nm	chalcocite Cu ₂ S	–		

Table 1. continued								
Exp. Approach	Metal source	IL	Sulfur Source	Exp. Parameters	Morphology	Crystal Structure	E_g	Ref
Electro-deposition	PbCl ₂	OLAHS	OLAHS	34 h, 160 °C (dissolving) → 20 min, RT	spherical NP, 5–7 nm	galena PbS	–	
	Bi(OCOC(CH ₃) ₂ (CH ₂) ₅ CH ₃) ₃	OLAHS	OLAHS in MSTL	2 h RT, stirring, add Acetone → 6h RT	nanowires	bismuthinite Bi ₂ S ₃	–	
	Cu(TFSI) ₂	(EMIm)TFSI	S ₈	WE: Pt disk, CE: Pt foil, RE: Ag wire 50 mV s ⁻¹	Stacked flake morphology (120 °C 50 nm), round particles (200 °C)	covellite CuS	–	[156]
	Cu(TFSI) ₂	[EMIm]TFSI	S ₈	120 °C, 1 h, –0.25 V, WE: Pt disk, CE: Pt foil, RE: Ag wire	NP (50–100 nm, 1 μm thick)	cubic Co ₉ S ₈ (<i>Fm3 m</i>)	–	[157]
	Cu(TFSI) ₂	[EMIm]TFSI	S ₈	120 °C, 1 h, –0.85 V, WE: Pt disk, CE: Pt foil, RE: Ag wire	Irregular shaped particles (3–5 μm)	Pyrite FeS ₂ , Marcasite FeS ₂	–	
	GeCl ₄	PP _{1,3} TFSI	HS(CH ₂) ₄ SH	RT, 10 min, –2.7 V, WE: GC, CE: Pt Wire, RE: Ag Wire	Porous structure with spherical particles (2–5 μm)	GeS _x monoclinic and amorphous GeS ₂	–	[158]

Estrada et al. described the synthesis of copper sulfide nanocrystals using an IL as the solvent, while injecting a single-molecule metal-sulfur-precursor.^[112] The results show the successful formation of copper sulfide nanoparticles with a monodisperse size distribution, which changes with varying temperatures. In all cases, the size distribution of the nanoparticles is below 50 nm. Additionally, Estrada et al. showed that the reaction temperature directly impacts and influences the crystal structure of the compounds by demonstrating that, depending on the reaction conditions, both cubic and rhombohedral digenite (Cu_{1.8}S), as well as monoclinic djurleite (Cu_{1.94}S) can form. The direct optical band gap changes with varying crystal structure with reported values of 1.4 eV (djurleite) and 1.75 eV (digenite).

Abouserie et al. described the successful synthesis of CuS (covellite) using bis(trimethylsilyl)sulfide, (TMS)₂S, which is directly injected into the pre-heated MIL bis(*N*-dodecylpyridinium) tetrachloridocuprate(II) (C₁₂Py)₂[CuCl₄].^[113] In this approach, the MIL functions as the solvent, the metal precursor, and the template guiding morphological and size evolution. So far, the resulting nanoparticles are hexagonal plates, with a rather broad size distribution ranging from 30 to about 700 nm. Platelike morphologies are consistent with previous work showing that (1) the MIL forms an organized (lamellar) reaction matrix and (2) has also previously favored the formation of nano- to microplate crystals.^[123,159,160]

In a recent study, the same authors have shown that not only CuS, but also CuCo₂S₄ can be made using a closely related approach.^[114] The advantage of the approach is that the bimetallic ILP, (C₄Py)₂[Cu_{0.39}Co_{0.61}Cl₄], is a precursor for CuCo₂S₄ (carollite) nano- and microparticles eliminating the need for two

individual precursors (Cu and Co precursor). A second advantage is that the Cu/Co ratio in the final metal sulfide particles is essentially identical to the Cu/Co ratio in the ILP. Moreover, the materials exhibit a very high efficiency in the electrocatalytic oxygen evolution reaction (OER). This latter feature is largely due to the high electrochemical surface area and the large number of catalytically active sites on the particle surfaces. While the reason for the high electrochemical surface area is not clear yet, it may likely stem from a very specific interaction of the IL template/precursor with the growing metal sulfide nanoparticles.

Besides these studies, we have recently evaluated two further heating up approaches, which will briefly be summarized here. First, we have studied the reaction of sodium thiosulfate with (C₄Py)[Cu_{0.50}Mn_{0.50}Cl₄]. The amount of sodium thiosulfate added to the reaction has a direct influence on the amount and the type of metal sulfide formed (Figure 6). EDX data shows that during reactions where 0.55 and 1.1 equivalents of Na₂S₂O₃ were used, only CuS was formed and no Mn could be observed in the final products, Table 2. Manganese can only be found in products of reactions, where the amount of the sulfur source exceeded the amount of the MIL by at least 1.5 times. EDX data also show the presence of oxygen even after purification. XRD data agrees very well with that of typical CuS (covellite, JCPDS No. 79-2321 ICSD 98-006-7581), while the reflections do not match up with MnS (alabandite, JCPDS 01-1089, ICSD 98-001-8007) or MnS₂ (hauerite, JCPDS 25-0549, ICSD 98-003-6545).^[161–163]

We currently hypothesize that the Mn is bound in the CuS forming Cu_{1-x}Mn_xS. Indeed, XRD data shows that between 1.0–1.5 and then from 1.5 to 2.0 equivalents of Na₂S₂O₃ used in the

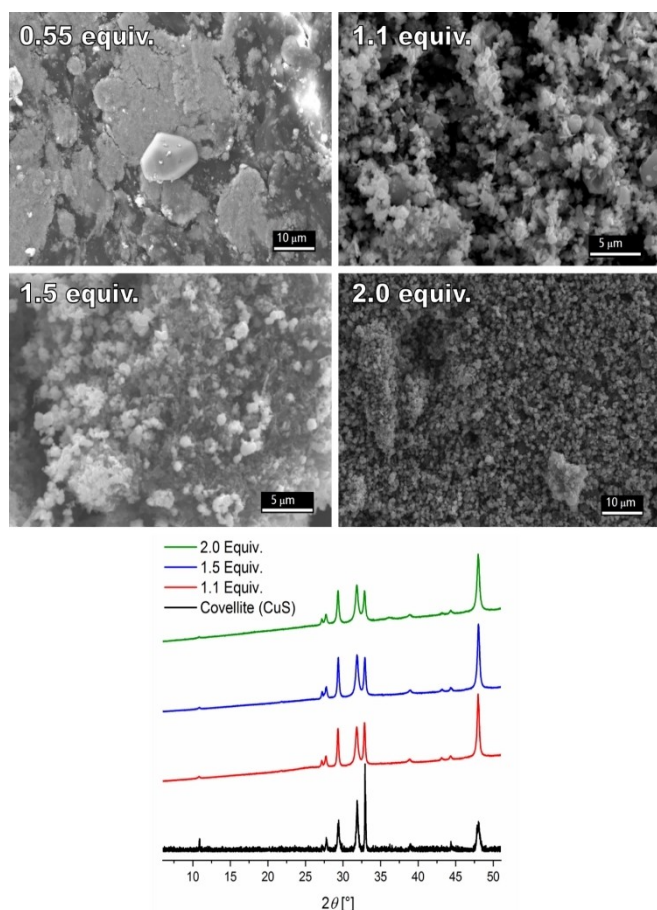


Figure 6. SEM and XRD data of metal sulfides synthesized by reaction of MIL with varying amounts of $\text{Na}_2\text{S}_2\text{O}_3$ (0.55 to 2.0 equivalents referring to the IL). In all cases, metal and sulfur precursors were ground and then heated up in a round flask to 190°C for 6 h without any other solvent. XRD data were collected using a PANalytical Empyrean powder X-ray diffractometer operating at 40 kV and 40 mA. The diffractometer was configured with a focusing X-ray mirror for Cu radiation ($\lambda = 1.5419 \text{ \AA}$) and a PIXcel1D detector. Scans were run for 61 min over a 2θ range of $4\text{--}70^\circ$ with a step size of 0.01318° .

Table 2. EDX data of metal sulfides obtained by the reaction of MIL with varying amounts of $\text{Na}_2\text{S}_2\text{O}_3$. SEM and EDXS experiments were done on a JEOL JSM-6510 with a W filament operated at 15 kV and equipped with an Oxford Instruments INCAx-act detector. Bulk samples were deposited on a carbon glue pad followed by sputtering with carbon using a Polaron CC7650 Carbon Coater. The Back Scattered Electron (BSE) detector was used for material contrast, the Secondary Electron (SEE) detector for topographic images at 15 kV.

Sample	Cu [atom%]	Mn [atom%]	S [atom%]	O [atom%]
0.55 equiv.	34.4	–	53.1	8.7
1.1 equiv.	38.8	–	61.2	–
1.5 equiv.	19.8	0.7	68.1	9.5
2 equiv.	18.5	7.7	65.0	7.5

reaction mixtures, the maxima of the main reflections shift by around $0.02\text{--}0.03$ degrees 2θ . This suggests a slight change in the unit cell volume of ca. 0.5 \AA^3 . Possibly, this indicates that some Cu^{2+} is substituted with Mn^{2+} . The presence of O in the EDX spectra possibly also indicates that either not all thiosulfate is decomposed or that some fraction of the product may also

be a $\text{Cu}_{1-x}\text{Mn}_x(\text{S}_{1-y}\text{O}_y)$ compound. There is, however, no oxide species that can be identified from the XRD data. Overall, a clear answer to these question will need more detailed X-ray data possibly supported by EXAFS or XPS measurements.

In a further study, we have also investigated the reaction of oleylamine-sulfur with $(\text{C}_4\text{Py})_2[\text{CuCl}_4]$.^[63] In this reaction, relatively homogenous Cu_xS nanoparticles were synthesized by the heating up method at the relatively low temperature of 140°C (Figure 7). TEM shows that the average size of the particles is $63.8 \pm 36.3 \text{ nm}$ and the particle size distribution is rather uniform. The optical band gap as determined by photoelectron spectroscopy and Tauc plot analysis is 2.64 eV and the HOMO level is 4.35 eV . The UV/Vis data show an increase of a long wavelength absorption at over 700 nm . Samples prepared at 60°C show a low absorption, while samples prepared at 140°C show an intense and very broad absorption at these long wavelengths. Samples prepared at even higher temperatures show again a rather low absorption. Possibly, this change in the optical properties vs. synthesis temperature is related to a structural transition as described previously.^[114,164]

Lastly, Tshemese et al. reported the synthesis of lead sulfide nanoparticles using a dual source precursor method, as well as a single molecule precursor method.^[145] For the dual source precursor method, lead acetate and the IL 1-ethyl-3-methylimidazolium methanesulfonate ($\text{EMIm}(\text{CH}_3\text{SO}_3)$) were used as the metal precursor and the reaction medium and solvent, while the sulfur precursor dodecanthiol or sodium sulfide was injected into the solution. This resulted in cubic and hexagonal galena nanoparticles ranging from 45 to 86 nm , while using dodecanthiol, and rectangular, spherical and branched monodisperse galena nanoparticles with a size of around 38 nm , while using sodium sulfide. For the single source precursor method, a lead ethyl xanthogenate complex ($\text{Pb}(\text{S}_2\text{COCH}_2\text{CH}_3)_2$) was injected into the preheated IL. This process produced cubic and hexagonal galena nanoparticles, with sizes ranging from 55 to 160 nm . Tshemese et al. also demonstrated that with increasing temperature, the size distribution of the particles also increases.

As stated in chapter 2 above for the synthesis in molecular solvents, another frequently used and popular synthetic approach is the heating-up method. Here, the different starting materials are brought together in a solvent and then collectively heated to start product formation. Biswas et al. report the successful synthesis of lead sulfide nanoparticle using lead acetate as a metal precursor, the IL 1-butyl-3-methylimidazolium tetrafluoroborate (BMImBF_4) as a solvent and reaction medium, and thioacetamide (TAA) as a sulfur precursor.^[146] The resulting particles are cubic galena (space group $Fm\bar{3}m$) with diameter of 10 nm and a monodisperse and narrow size distribution.

In a direct comparison between heating-up and hot injection, Estrada et al. reported that various copper sulfide nanoparticle phases are not dependent on the temperature profile during synthesis, since both hot injection and heating up method result in the same phases provided that the final temperature and the solvent are the same in both cases.^[112] Thus, both digenite ($\text{Cu}_{1.8}\text{S}$) and djurleite ($\text{Cu}_{1.94}\text{S}$) phases in the

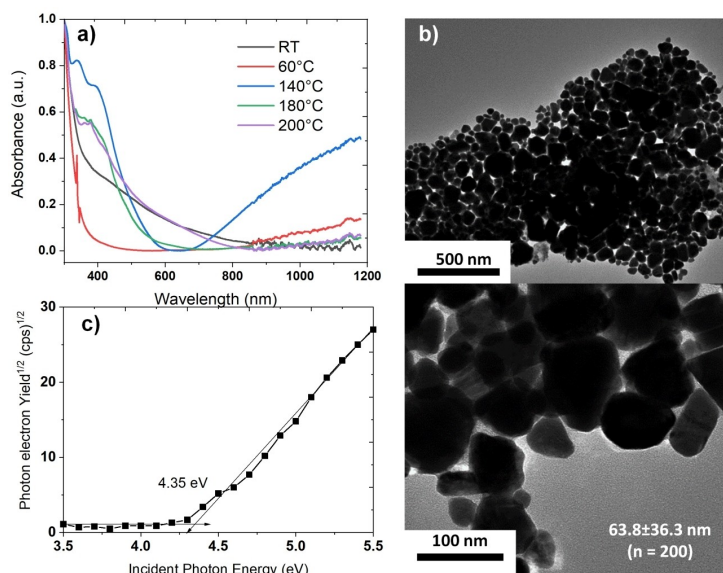


Figure 7. a) UV/Vis spectra of Cu_xS nanoparticles made by reaction of (C₄Py)₂[CuCl₄] with oleylamine-sulfur at different reaction temperatures. b) TEM image of Cu_xS nanoparticle obtained by reaction at 140 °C. c) Photoelectron spectrum of Cu_xS nanoparticles produced at 140 °C. UV/Vis spectroscopy was done on a Perkin Elmer Lambda 19 UV/Vis/NIR. TEM was done on a JEOL JEM-1400Plus operated at 200 kV, photoelectron spectroscopy was done on a Nikkan AC-2 PESA using excitation energies from 3.5 to 6.2 eV.

form of rhombohedral or cubic and monoclinic nanocrystals can be synthesized using a batch heating up method.

Unlike the experimental approaches described above, which revolve around temperature control in liquid phase reactions, typical inorganic solid-state reactions rely on mechanical preparation of the solid precursors prior to starting the (high temperature) solid state reaction. Those include, for example, grinding or milling followed by high temperature treatment. However, there appear to be no current examples using ILs at the moment. Likely, this is due to the fact that higher temperatures also lead to degradation of the organic components of the IL producing carbonaceous materials but not the pure metal sulfide nanoparticles.

In contrast to high temperature reactions, metal sulfide syntheses via mechanochemical procedures, which do not involve ILs, are widely known. Tsuzuki et al. showed the successful synthesis of different transition metal sulfides using the respective chlorides as metal precursors, as well as calcium sulfide and sodium sulfide as sulfur precursors.^[106,147] The materials were ground under argon in a steel ball mill. The syntheses resulted in cubic zinc sulfide (zinc blende/sphalerite) nanoparticles ranging from 6 to 30 nm, hexagonal and cubic cadmium sulfide (wurtzite/sphalerite) nanoparticles ranging from 4 to 8 nm, and tetragonal and cubic cerium sulfide (β -Ce₂S₃, γ -Ce₂S₃) nanoparticles with a size of 8 to 13 nm.

Tolia et al. reported the synthesis of metal sulfides using the same mechanochemical approach involving grinding the respective materials.^[107] The respective (transition) metal acetates functioned as the metal precursors, while sodium sulfide acted as the sulfur precursor. The materials were ground for 2 to 10 h under argon in a steel ball mill. The syntheses resulted in hexagonal zinc sulfide (sphalerite, wurtzite) nanoparticles

ranging from 2 to 5 nm, cubic lead sulfide (galena) nanoparticles ranging from 8 to 25 nm, cubic and hexagonal cadmium sulfide (hawleyite and greenockite) nanoparticles ranging from 8 to 13 nm, and agglomerated copper sulfide (covellite) nanoparticles ranging from 6 to 8 nm. ILs have indeed also been used in mechanochemical syntheses in the last couple of years, as shown by the use of the terminus “ionic liquid assisted grinding (ILAG)”, although so far not many details on the process have been published.^[165,166]

Furthermore, ultrasound-assisted reactions have been used in IL-based nanoparticle syntheses. The main advantage of sonochemical approaches is the extreme reaction parameters created by acoustic cavitation involving the formation, growth, and implosive collapse of bubbles in liquid phases, which influence the formation of nanoparticles.^[167] For example, Goharshadi et al. demonstrated the successful synthesis of zinc sulfide nanoparticles using sonochemistry.^[148] Here, a variety of 1-alkyl-3-methylimidazolium bis-(trifluoromethylsulfonyl)-imide ((C_xMIm)NTf₂, x = 4–8) ILs were used as the solvent and reaction medium in connection with distilled water. Zinc acetate and thioacetamide functioned as the respective metal and sulfur precursors. The mixture was held at 60 °C for 15 min under stirring, using a frequency of 20 kHz and a total acoustic power of 44 ± 0.5 W. The synthesis resulted in cubic zinc sulfide nanoparticles with a size of 12 nm and a band gap ranging from 4.86 to 5.77 eV.

Similarly, Garcia-Gomez et al. reported the sonochemical synthesis of tin sulfide nanoparticles using tin chloride and thioacetamide as the precursor materials.^[115] The IL (BMIm)BF₄ and ethanol were used as the solvents. The reaction was done at room temperature using a frequency of 20 kHz and a total acoustic power of 100 W. Polygonal and spherical tin sulfide

(orthorhombic herzenbergite) with a size of 350 to 450 nm and a band gap of 1.8 eV were obtained. The authors also report that the use of an ethanol-IL-mixture instead of the pure IL increases the crystallinity of the product.

In the same manner, Barzegar et al. successfully synthesized cadmium sulfide nanoparticles.^[149] Again, the corresponding metal acetate and thioacetamide were used as the precursor materials. A mixture of 1-ethyl-3-methylimidazolium ethylsulfate (EMIm)(EtSO₄) and distilled water was the reaction medium and solvent. The reaction took place at room temperature for 60 min with a frequency of 23 kHz, a total acoustic power of 140 W, and under magnetic stirring. The authors describe a significant impact of the water on the reaction outcome. While the use of distilled water leads to the growth of slightly bigger (nearly) spherical cadmium sulfide (cubic hawleyite) nanoparticles with a size of 5 to 6 nm, those particles seem to be slightly less agglomerated. In contrast, the use of pure IL leads to the growth of marginally smaller nanoparticles with a size of 3 to 5 nm, which seem to be slightly more agglomerated. In both cases, the resulting nanoparticles have a band gap of 2.42 eV.

Besides ultrasound-assisted synthesis, microwave-assisted syntheses protocols have been popular for nanoparticle synthesis. The main advantages of microwave chemistry are high reaction rates, rapid heating, dramatic decrease of reaction time, and increase of yield.^[150]

In contrast to more traditional approaches like oil bath heating, microwaving leads to heat being produced mostly inside the reaction vessel rather than induced externally via oil baths or heating mantles. Dipolar polarization and ionic conduction triggered by microwave irradiation leads to increased particle migration and movement due to their electric and magnetic components, which results in a higher number of collisions and friction among the molecules.^[152,168]

ILs have proven as successful reaction media and additives, since (as a result of the presence of large positively charged organic ions with high polarizability and the overall high ionic conductivity in ILs) they are excellent absorbers for microwaves.^[150-152] The combination of microwaves with ILs therefore provides a simple yet powerful tool for materials synthesis.

For example, Jiang et al. reported the successful synthesis of bismuth(III) sulfide and antimony(III) sulfide nanoparticles.^[150] The respective oxides were used as metal sources and sodium thiosulfate was used as the sulfur source. A mixture of the IL (BMIm)BF₄ and ethylene glycol or ethanolamine, as well as hydrochloric acid (37 wt%), was used as the reaction medium. For bismuth(III) sulfide nanoparticles the reaction was held at 190 °C for 30 s or 10 min, while for antimony(III) sulfide nanoparticles the synthesis was done at 165 °C for 40 min. Regarding the Bi₂S₃ nanoparticles, the synthesis resulted in single-crystalline nanorods (orthorhombic bismuthinite) with a length of about 80 nm after 30 s of microwaving and 60 nm after 10 min of microwaving. Interestingly, the authors also report that the presence of the IL leads to longer and thinner nanorods and suggest that it may function as a surfactant during the formation of the structures. The synthesis of Sb₂S₃ nanoparticles

also resulted in single-crystalline nanorods (orthorhombic stibnite) with a length of about 3 μm and diameters of 200 nm. The authors also describe a significant influence of the IL on the morphology of the nanoparticles.

Furthermore, Jiang et al. also reported the synthesis of zinc sulfide and cadmium sulfide nanoparticles in a previous article.^[151] In this study, zinc acetate and cadmium chloride were used as the respective metal sources. In both cases, the metal precursor was dissolved in (BMIm)BF₄ and heated to 100 °C, before an aqueous sodium sulfide solution was added. The reaction mixture was held at 100 °C for 10 min under magnetic stirring and resulted in cubic ZnS (zinc blende, sphalerite) and hexagonal CdS (greenockite). In both cases spherical nanoparticles with an average size of 3.5 nm (ZnS) and 7 nm (CdS) were produced.

Similarly, Esmaili et al. synthesized spherical zinc sulfide nanoparticles using microwave synthesis.^[152] While zinc acetate provided the necessary metal ions, thioacetamide (TAA) was used as the sulfur source and a mixture of (EMIm)(EtSO₄) and water functioned as the reaction medium. The precursors were dissolved in the IL and irradiated for 4 min at 55% power output at room temperature. The synthesis also resulted in cubic zinc sulfide (zinc blende/sphalerite) nanoparticles with a spherical shape and a size of approximately 2.4 nm. The authors furthermore report that the nanocrystalline ZnS particles aggregate to clusters ranging from 200 to 1000 nm, with a decreased particle size with an increased IL content of the solvent. The resulting nanoparticles have an increased band gap of 3.90 eV compared to bulk ZnS, which according to the authors is a result of the quantum confinement in nanocrystalline ZnS.

In line with the two aforementioned synthetic approaches, which rely on different physical phenomena to create extreme reaction conditions, autoclave-chemistry is a well-known and common experimental route used to create nanoparticles. Here, extreme reaction parameters like high temperature and high pressure are produced within the autoclave restricting the reaction volume. Hydrothermal and solvothermal approaches have been discussed above, but the analogous ionothermal reactions shall be discussed now.^[169-174] Ionothermal reactions share a number of features with hydro- or solvothermal reactions but are different in the sense that the pressure in ionothermal reactions is often lower and that thermal conductivities and thermal conditions in these reactions are often not directly comparable.

Using an ionothermal approach, Ruck et al. made a series of metal sulfides, including PbS, CdS, Ag₂S, ZnS, Bi₂S₃, Sb₂S₃ and CuS.^[153] A series of metal acetates (Pb, Cd, Sb) and nitrates (Ag, Zn, Bi, Cu) functioned as the respective metal precursors, while a mixture of choline chloride (ChCl) and thioacetamide (TAA) functioned as the sulfur source and a deep eutectic solvent analogous to ILs. In all cases, the metal salts were dissolved in the TAA/ChCl mixture at 70 °C and then transferred into an autoclave, where the reaction was held at 150 °C or 180 °C for 15 h. Although the pressure was not increased on purpose by the authors, it did exceed 1 atm over the course of the reaction. The authors did not comment on the reasons. As stated above,

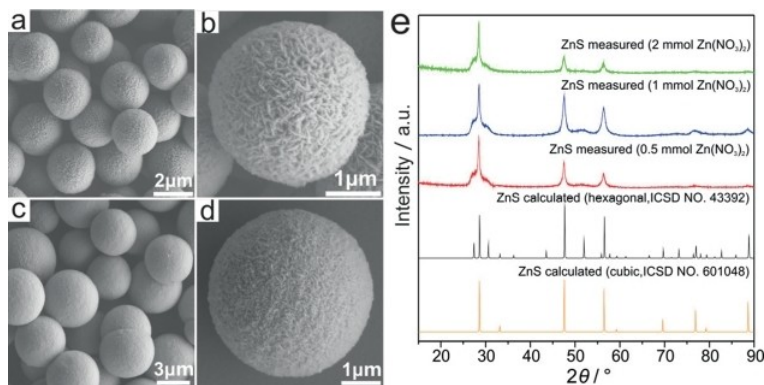


Figure 8. Morphology and structure of the synthesized ZnS microspheres by Ruck et al. Picture a) to d) show SEM images of the ZnS synthesized with varying amounts of the metal precursor. e) shows a comparison of the measured and calculated XRD data of the microspheres. Image reprinted with permission from Ruck et al. *Z. Anorg. Allg. Chemie*, 643: 1913–1919.^[153]

however, it must clearly be noted that the pressures are much lower than what is common in regular solvothermal reactions.

The reactions involving the metal acetates resulted in polyhedrally shaped monoclinic Ag_2S (acanthite, $P2_1/n$) particles ranging from 2 to 8 μm , cubic and hexagonal ZnS platelets and microspheres (sphalerite and wurtzite) ranging from 200 nm to 4.5 μm , orthorhombic Bi_2S_3 (bismuthinite, $Pnma$) microflowers composed of nanowires with a size of 30 nm, and hexagonally shaped CuS plates (covellite, $P6_3/mmc$) ranging from 20 to 70 μm , (Figure 8). Reactions starting from the respective metal nitrates resulted in octahedrally shaped cubic PbS (galena) crystals with a size of 300 nm, spherically shaped hexagonal CdS (greenockite type, space group $P6_3mc$) with a size of 30 nm, and stacked orthorhombic Sb_2S_3 sheets (stibnite, $Pnma$) with a size of 50 nm.

In a further study, Ge et al. reported the successful synthesis of hollow CuS spheres using an ionothermal approach.^[154] Here, CuCl_2 was used as metal source, while a mixture of sulfur powder (S_8) and carbon disulfide (CS_2) functioned as the sulfur source. The IL (BMIm) BF_4 acted as the solvent. After the precursor materials were dissolved in the IL, the reaction flask was sealed in an autoclave and the reaction was held at 130 $^\circ\text{C}$ for 24 h. The synthesis resulted in nestlike hollow spheres of hexagonal CuS (covellite, $P6_3/mmc$) consisting of flakelike microcrystallites, with a size of 5 to 8 μm . The authors highlight the morphology-controlling effect of the IL by showing that microspheres could only be obtained with (BMIm) BF_4 . The authors also describe a distinct blue-shift of the absorption behavior of the CuS spheres, which they attribute to the quantum size (or quantum confinement) effect. Figure 9 shows a schematic illustration of the proposed formation mechanism.

Additionally, Biswas et al. reported the successful synthesis of ZnS and CdS nanoparticles while investigating the effect of the IL on the morphology.^[146] The authors used the respective metal acetates as the metal source and thioacetamide (TAA) as the sulfur source in combination with the ILs (BMIm) BF_4 , (BMIm)(MeSO_4), and (BMIm) PF_6 . The precursor materials and the IL were sealed in an autoclave at 180 $^\circ\text{C}$ and the reaction was held at this temperature for 5 h. The synthesis involving zinc

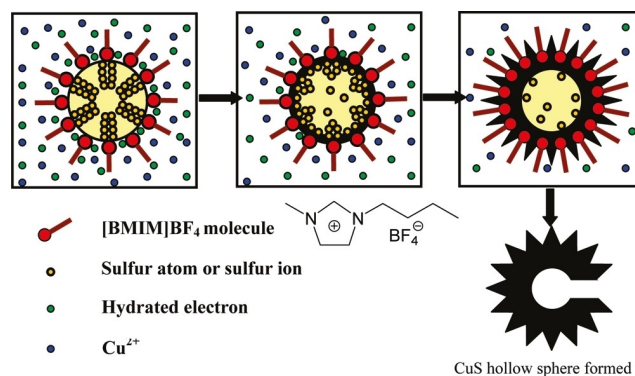


Figure 9. Proposed formation mechanism of CuS hollow microspheres by Ge et al. Reprinted (adapted) with permission from Ge et al., *Crystal Growth & Design*, 2010, 10, (4), 1688–1692.^[154] Copyright 2010 American Chemical Society.

acetate resulted in hexagonally shaped ZnS plates (wurtzite, $P6_3mc$) with a size of 3 nm. Analogous reactions with cadmium acetate resulted in hexagonal CdS nanoparticles (space group $P6_3mc$) with sizes between 4 and 13 nm and the nanoparticle size strongly depends on the anion of an imidazolium-based IL, an effect that has also been shown for gold nanoparticles.^[175]

Moreover, a well-known and thoroughly studied experimental approach is precipitation. Precipitation is a very popular and simple synthesis route, since it usually does not need extreme reaction conditions. Using this approach, Fan et al. successfully synthesized CuS nanoparticles.^[155] The authors used a mixture of 1-butyl-3-carboxymethylimidazolium bis(trifluoromethylsulfonyl)imide ($\text{C}_4\text{C}_2\text{OOHIm}$) NTf_2 and water, along with 1-methylimidazole, as the solvent and the reaction medium. The 1-methylimidazole also acted as a complexing ligand to ensure the transfer of the copper ions into the IL phase. In separate syntheses, TAA and Na_2S functioned as the respective sulfur source, while a $\text{Cu}(\text{OAc})_2$ solution acted as the metal precursor. In all cases, the water phase of the copper acetate solution was removed after mixing to remove the undissolved $\text{Cu}(\text{OAc})_2$. Afterwards, the sulfur source was added to the IL mixture under stirring for 15 min. The reaction took

place at room temperature when Na_2S was used, or at 80°C with TAA. After a color change indicated the formation of CuS , ethanol was added to dissolve the IL phase to precipitate CuS . The synthesis involving Na_2S resulted in self-assembled large plate-like nanostructures. The authors did not provide the size distribution of the nanoparticles because the particles tend to agglomerate to a large extent, but TEM images suggest that the nanoparticles are smaller than 200 nm. Synthesis involving TAA resulted in rough and spheroidal nanostructures. Again, the size distribution was not described due to agglomeration, but TEM images suggest a size below 50 nm, while SEM images show a rather polydisperse size distribution of both the nanoparticle and the aggregates.

Additionally, Yuan et al. reported the successful syntheses of multiple metal sulfide nanoparticles, including Ag_2S , Cu_2S , PbS , Bi_2S_3 , and $\text{Au}@/\text{Ag}_2\text{S}$ Janus particles, using the precipitation route.^[65] Different metal salts, including acetates and nitrates, were used as metal sources, while the IL oleylammonium hydrosulfide (OLAHS) was used as the sulfur source and the reaction medium or solvent. Mostly, mesitylene was added to OLAHS to decrease the viscosity and facilitate handling at room temperature. The synthesis resulting in Ag_2S involved AgNO_3 , which was dissolved in oleylamine (OLA) and toluene, before OLAHS was added under stirring in air at room temperature and the mixture was stirred for about 60 min producing monodisperse Ag_2S nanoparticles (acanthite, $P2_1/n$) with a diameter of 8 to 9 nm.

The authors also describe the synthesis of $\text{Au}@/\text{Ag}_2\text{S}$ Janus nanoparticles, which involved silver acetate and previously made gold nanoparticles dissolved in OLA and toluene. The reaction was held at 80°C for 10 min before H_2S was added at room temperature to form OLAHS *in situ*. This resulted in monodisperse nanoparticles with a diameter of 8 to 9 nm. The synthesis of Cu_2S nanoparticles involved copper(I) acetate, which was dissolved in OLA and heated to 80°C to ensure the metal precursor is completely dissolved. Then, OLAHS in mesitylene was added and the reaction was held at room temperature for 26 h. The Cu_2S nanoparticles were precipitated

using acetone. The synthesis resulted in spherical Cu_2S nanoparticles (chalcocite) with a size of 4 to 7 nm.

To produce PbS nanoparticles, PbCl_2 was mixed with OLA and toluene was added. Afterwards, H_2S was added under mechanical stirring to form the OLAHS *in situ* and the reaction was held at room temperature for 35 min. The synthesis resulted in spherical PbS nanoparticles (galena) with a diameter of 5 to 7 nm. Lastly, Bi_2S_3 nanoparticles were successfully synthesized using OLAHS in mesitylene, which was injected in a mixture of OLA and bismuth neodecanoate ($\text{Bi}(\text{OCOC}(\text{CH}_3)_2(\text{CH}_2)_5\text{CH}_3)_3$) under stirring and the reaction was held at room temperature for 2 h. As a result, Bi_2S_3 (bismuthinite, $Pnma$) nanowires were successfully produced. Figure 10 illustrates the approach and compares it to more traditional approaches involving H_2S .

Lastly, another approach, which is increasingly becoming popular, is electrodeposition. This approach is based on the movement and deposition of charged particles influenced by an electric field onto a conductive electrode, which leads to a coherent coating and films of varying thicknesses.^[176] The main advantages of this approach are the high purity of the synthesized films, the wide range of materials this can be applied to, the uniformity of the coatings, the relatively high speed of the process, and the easy control of the composition.^[177]

By using an electrochemical route, Chen et al. reported the successful synthesis of CuS nanoparticles. Copper(II) bis(trifluoromethanesulfonyl)imide ($\text{Cu}(\text{TFSI})_2$) was used as the metal source, while elemental sulfur functioned as the sulfur source.^[156] The IL (EMIm)TFSI acted as the solvent and reaction medium. Both precursors were first dissolved in the IL to create the electrolytic bath. Afterwards, platinum working and counter electrodes were used alongside a silver reference electrode. The reaction temperature was initially 120°C and later increased to 200°C . The synthesis resulted in stacked flake-like CuS nanoparticles (covellite, $P6_3/mmc$) at 120°C with a width of $1\ \mu\text{m}$ and a thickness of 50 nm, and in round CuS nanoparticles (covellite, $P6_3/mmc$) at 200°C with sizes under $1\ \mu\text{m}$.

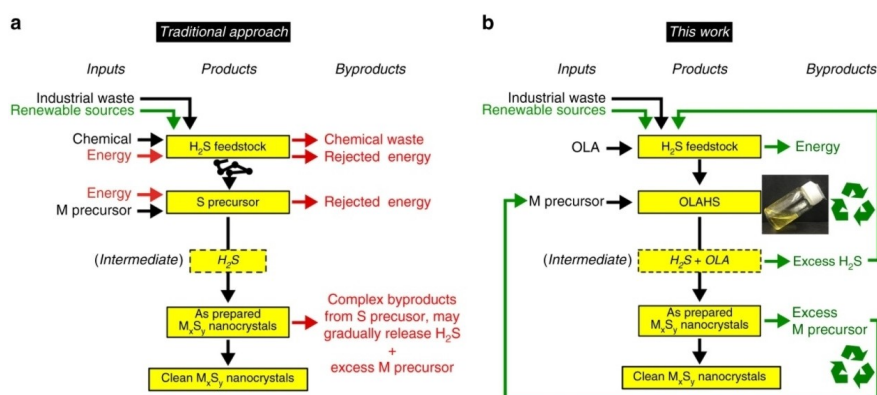


Figure 10. Comparison of educts and products for metal sulfide nanoparticle syntheses using a) traditional approaches and b) the OLAHS-approach developed by Yuan et al.^[65] M and S stand for metal and sulfur respectively, while M_xS_y describes a metal sulfide compound. The labeling the black boxes “traditional approach” and “this work” refer to the original article and are part of the original figure.

Additionally, Chen et al. successfully synthesized CoS and FeS nano- and microparticles using electrodeposition.^[157] Here, cobalt(II) bis(trifluoromethanesulfonyl)imide (Co(TFSI)₂) and anhydrous iron(III) chloride were used as the metal precursors and elemental sulfur was used as the sulfur source. Again, the IL (EMIm)TFSI was used in the electrolytic bath as the solvent for both precursor materials and reaction medium. A typical three-electrode-setup was used, consisting of Pt working and counter electrodes and a silver reference electrode. The electrodeposition reactions were done at 120 °C for 60 min at −0.25 V and −0.85 V, respectively. As a result, irregularly shaped cobalt sulfide nanoparticles (cubic Co₉S₈, *Fm3m*) with sizes between 50 and 100 nm, and irregularly shaped iron sulfide microparticles (cubic pyrite, *Pa3*, and orthorhombic marcasite, *Pnm*) with sizes between 3 to 5 μm were obtained.

Furthermore, Murugesan et al. reported the successful synthesis of germanium sulfide particles using electrodeposition.^[158] Germanium chloride (GeCl₄) and 1,4-butanedithiol served as the metal and sulfur precursor materials, while *N*-methyl-*N*-propylpiperidinium bis(trifluoromethanesulfonyl)imide (PP_{1,3})TFSI was used as the solvent and reaction medium. A glassy carbon working electrode and a platinum counter electrode was used alongside a silver quasi-reference electrode. The electrodeposition was done at room temperature for 10 min at −2.7 V. The reaction resulted in a porous structure with spherical particles consisting of germanium sulfide (GeS_x, monoclinic and amorphous GeS₂) with particle sizes between 3 to 5 μm.

In summary, ILs have provided a number of interesting approaches and materials but the nucleation, growth, and final product formation are not always straightforward and more details about the formation of metal sulfides from ILs are necessary to develop a rational design approach. This includes advanced experimental and theoretical tools.

4. Computational Tools for Understanding Particle Formation and Structure

The toolbox of theoretical and computational chemistry can support the experimental procedure by answering questions where the empirical data is missing or unavailable. Arising controversies in empirical results can be pointed out and can be clarified by theoretical chemistry, e.g., by providing otherwise unavailable data. Hence, computational chemistry can yield important insights helping the design of synthetic materials.

The role of computational chemistry can be split into the need of achieving physical properties through the (1) design of a target nanoparticle, the (2) synthetic approach and experimental conditions – in order to realize the material with the desired properties – and the (3) characterization of the nanoparticles produced by the synthesis route.

Firstly, the application of a targeted nanoparticle is strongly correlated to the necessity of fulfilling characteristic demands of the chosen application. As an example, in the case of a solar

cell with a single p-n junction, the major goal is the design of a nanoparticle with an optical bandgap close to the Shockley-Queisser limit of 1.34 eV.^[178] An area in which density functional theory (DFT) has had a long history of impact is the bandgap and solving the bandgap problem with hybrid functionals or many-body theory approaches like GW.^[179-181] Hence a prediction and screening of the bandgap of pure and mixed bulk metal sulfide nanoparticles is accessible through computational chemistry (database: materials project) or theoretical chemistry (advanced DFT calculations).^[182,183] Table 3 shows relevant examples of the computed direct bandgaps of bulk ternary sulfides where the properties were calculated on the DFT (generalized gradient approach, GGA) level without spin-orbit coupling. The magnetic anisotropic energy (MAE) is about 0.6 eV due to the low level of theory used in the database which tends to underestimate the bandgap. Therefore, some compounds are predicted to be metallic, even if they are not.

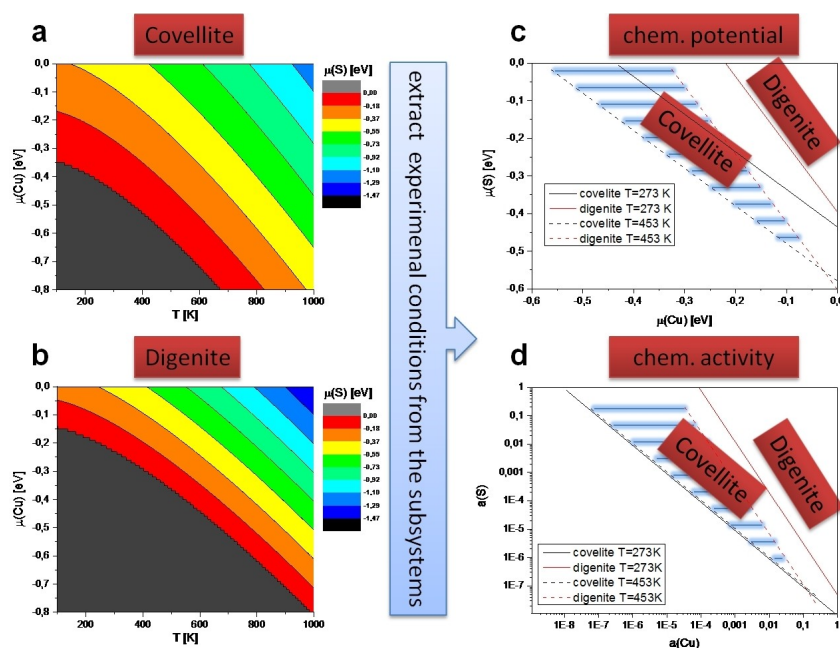
In terms of nanoparticles, the quantum size effect has a major impact on the optical properties. This is due to the confinement effect, which opens up the optical gap depending on the size of the particles. This can be included qualitatively in the design strategy. A more systematic method for the prediction of the optical gap of nanoparticles might be the use of ab initio calculations which, however, is quite expensive compared to other methods. Therefore, numerous research groups currently evaluate and implement heuristic models to address the question of calculating optical gaps of nanostructures bigger than a few nanometers.^[184-186]

Secondly, as described in chapter 1, typical synthetic protocols often include the use of high temperatures, thus leading to the thermodynamic products. Consequently, the information about the phase diagram of a multicomponent system is crucial for the prediction of the phase and structural outcome of the synthetic protocol under the chosen experimental conditions. Constructing a phase diagram manifesting the equilibrium thermodynamic properties of the system by assessing the thermodynamic properties of all the single phases in the system leads to a powerful tool to adjust the experimental conditions in a synthetic protocol regarding the temperature, pressure and chemical potential of the used precursors as it has been shown for the case of Cu₂ZnSnS₄ (CZTS) and Cu₂ZnSnSe₄ (CZTSe).^[187]

In contrast to the thermodynamic modeling that strongly depends on empirical data sets, ab initio thermodynamics can reveal all necessary variables of the subsystems to build a phase diagram on top of first principal calculations without the necessity of experimental data. This is shown in Figure 11 for the subsystems covellite and digenite and their thermodynamic behavior under different reaction parameters, specifically *T* and the activity *a* of the precursors. The DFT/time dependent DFT (TDDFT) calculations were done using an all electron numerical atom-centered orbital (NAO) basis set – on the tier 2 level – implemented in the FHI-aims code by using the Perdew-Burke-Ernzerhof (PBE) functional for geometry optimization, ground state energies and phonon calculations in the quasi harmonic level based on the supercell approach with the finite displacement method included in the phonopy package.^[188-190]

Table 3. Overview of calculated direct bandgaps on the level of DFT(GGA) for crystals with the composition $M_nM_2S_x$ ($M = \text{Mn, Cu, Zn, Cd}$) extracted from the materials project database. Bandgaps indicated with a * have been calculated without a band structure calculation and might be different in reality.^[183]

Formula	Space group	Crystal System	Formation Energy [eV]	E_g [eV]	Theoretical
Mn(CuS) ₂	F43m	cubic	-0.464	0.302*	TRUE
Mn ₂ ZnS ₄	Fd3m	cubic	-0.972	0	FALSE
Mn ₂ ZnS ₅	Pmmn	orthorhombic	-0.545	0*	TRUE
Mn ₄ CdS ₅	R3m	trigonal	-0.806	0*	TRUE
Mn ₄ CdS ₅	I4/m	tetragonal	-0.789	0	TRUE
Mn ₄ ZnS ₈	R3m	trigonal	-0.96	0*	TRUE
Mn ₄ ZnS ₈	R3m	trigonal	-0.933	0*	TRUE
MnCd ₂ S ₃	Cm	monoclinic	-0.932	0*	TRUE
MnCd ₄ S ₅	Cm	monoclinic	-0.952	0.609*	TRUE
MnCd ₄ S ₅	Cm	monoclinic	-0.95	0*	TRUE
MnCd ₄ S ₅	R3m	trigonal	-0.936	0.253*	TRUE
MnCdS ₂	P3m1	trigonal	-0.907	0.546	TRUE
MnCdS ₂	R3m	trigonal	-0.906	0.536	TRUE
MnZn ₃ S ₄	P3m1	trigonal	-1.064	0.548	TRUE
MnZn ₄ S ₅	Cm	monoclinic	-1.081	1.208*	TRUE
MnZn ₄ S ₅	P3m1	trigonal	-1.078	0.375*	TRUE
MnZnS ₂	P3m1	trigonal	-0.989	0.506	TRUE
MnZnS ₄	P21/c	monoclinic	-0.815	0*	TRUE
Zn ₃ CdS ₄	P43m	cubic	-1.085	1.68	TRUE
Zn ₄ CdS ₅	P3m1	trigonal	-1.083	1.546*	TRUE
Zn ₄ CdS ₅	R3m	trigonal	-0.809	0*	TRUE
ZnCd ₃ S ₄	P43m	cubic	-1.004	1.216	TRUE
ZnCdS ₂	P4m2	tetragonal	-1.04	1.369	TRUE
ZnCdS ₂	P3m1	trigonal	-1.024	1.328	TRUE
Mn(CuS) ₂	F43m	cubic	-0.464	0.302*	TRUE

**Figure 11.** Creating a phase diagram from ab initio thermodynamics with the subsystems of a) covellite and b) digenite by merging the information to show the stability window of covellite with respect to c) the chemical potential and d) the chemical activity of the precursors at the reaction temperature and the thermodynamic standard temperature.

The key quantity regarding the construction of a phase diagram is the study of a (T, p) ensemble of the Gibbs free energy G , by solving the equation shown in Figure 12. Calculations on the DFT level, which is the state of the art in computational material sciences, gives access to the electronic structure which lies in the time and length scale of the microscopic regime, whereas thermodynamic phenomena are

being covered in the meso- and macroscopic regime and are linked via the multiscale modeling approach which is described in detail elsewhere.^[191]

In the equation in Figure 12, the leading term of the total Energy E_0 is acquired by the electronic structure calculation for instance DFT, whereas the second term F_{vib} involves the contributions that occurs by vibration and includes the zero-

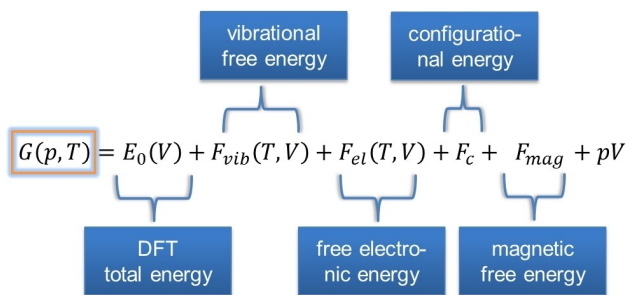


Figure 12. The Gibbs free energy as the key parameter in phase stability and phase diagram construction disentangled in the different contributions that can be calculated via ab initio DFT.

point energy and vibrational entropy. The finite displacement method or the linear response formalism are used to provide this information from a phonon frequencies analysis, based on a DFT calculation. The third term F_{el} accounts for the free electronic energy with the mixing contribution of the excited states into the ground state electronic structure and can therefore be calculated by TDDFT. Lastly, the configurational entropy F_c , the magnetic free energy F_{mag} , and the pV term play a significant role in calculating the Gibbs free energy under specific conditions (for alloys, magnetic systems and extreme conditions, respectively). Hence they can be neglected in the case of TMSs and are only shown in the equation for completeness.

Although DFT has become a standard tool for electronic structure calculations it has its limitations due to the fact that approximations are essential for in silico calculations. Considering thermochemistry, the fact that DFT is strictly only valid at $T=0$ K and $p=0$ atm has to be mentioned here. In spite of this, benchmark tests are available to classify the outcome of a DFT calculation, which is an advantage due to the fact that no computational gold standard for solids is available so far.^[192] Moreover, these drawbacks of DFT can be compensated by the benefit of the systematical improvement of the accuracy of DFT calculations (Jacob's ladder) and the fact that already reasonable results can be obtained for the formation enthalpies of TMSs, as described by Stevanovic et al. with an MAE of 0.05 eV/atom.^[193,194] Hence the quantifier of the equation shown in Figure 12, namely the formation enthalpy – which in a first

approximation is the DFT total energy – can be captured accurately within the DFT framework.

Last, the interpretation of other data obtained from TMS nanoparticles or from the IL precursors might be challenging due to the lack of comparable data. Especially XRD is a powerful technique to investigate the crystal structure and properties of nanoparticles, which in most cases cannot be classified to a single crystal structure. Modeling the crystal structure with electronic structure theory and the XRD patterns with the theoretical basis of solid-state physics (Bragg, Laue, and Fourier's theorems) are routinely described in literature.^[195] For instance, within this framework it is possible to simulate the diffractogram of a precursor used in the TMS nanoparticle synthesis as it has been done in the case of $[C_{12}Py]_2[CuCl_4]$ as shown in Figure 13.^[118]

5. Future Perspectives and Challenges

As stated in the sections 2 and 3 above, there is a large number of studies on metal sulfide nanoparticle synthesis and there is also a fairly good understanding of the properties of these materials. However, there is, like in many other materials synthesis fields, still a lack of control of individual bond formation in the sense that we know it from synthetic organic or macromolecular chemistry. While in these cases, there is a true molecular understanding of activation, reaction mechanisms, and product formation, including the respective thermodynamic and kinetic controls, the very same understanding is much more difficult for nanomaterials formation. Among others, this is due to the fact that in molecular chemistry there are many different types of bonds with specific properties, accessibilities, relative geometries, electronic details, etc. that make them different from most, if not all, other bonds in a given molecule.

In contrast, (nano)particle formation is largely controlled by stochastic events, in particular when considering the fact that a certain minimum of atoms or ions must meet to form a nucleus.^[196–199] Moreover, the formation of a nanoparticle or nanocrystal involves the formation of a large number of essentially identical or at least very similar chemical bonds. While still electronic, charge, and steric requirements must be met to form a nanoparticle, the specific differentiation of an individual bond vs. all other bonds surrounding this particular

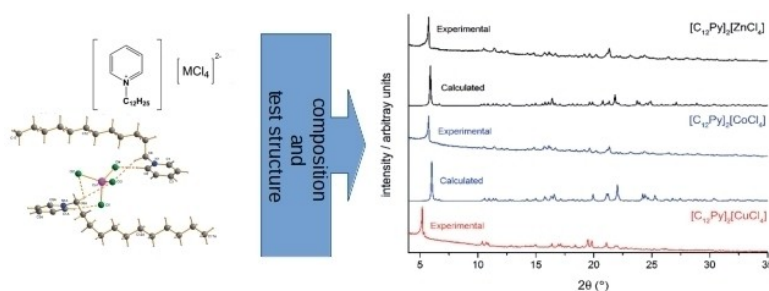


Figure 13. Example of modeling the XRD patterns by known compositions and a close enough test structure for an IL precursor used for the TMS synthesis.^[118]

bond is rather difficult to non-existent. In summary, this implies that we are still far from rationally designing inorganics a priori at the same level we are now able to do this for organic molecules. As a result, additional pathways and strategies towards new or improved nanoparticles are still important. It is therefore worthwhile considering, which advantages can be brought into a nanomaterials synthesis and design approach via ILs, ILPs, and related systems.

Clearly, ILs have advantages (or shall we say, different properties that may be useful) compared to conventional liquid phase synthesis. For example, ILs dissolve a number of compounds that cannot be dissolved otherwise or at least not under mild conditions. The most famous example likely is cellulose, but other organic and inorganic compounds have successfully been dissolved in ILs as well.^[200–203] A successful dissolution process of an otherwise insoluble compound clearly provides access to materials that cannot easily be made otherwise. For example, the synthesis of cellulose/inorganic composites is greatly enhanced by the fact that there are ILs that dissolve both the cellulose and the inorganic precursors. The resulting materials show high levels of complexity and often an ordered hybrid nanoarchitecture.^[204] Similar observations can, for example, also be made for silk fibroin/inorganic composites.^[205]

Moreover, ILs can provide very specific reaction environments, because they can provide strongly segregated domains with different characteristics of the individual domains. This includes ionic liquid crystal phases with highly polar ionic domains that are perfectly suited for (nano)crystal formation even at elevated temperatures.^[206–208] For example, various ILs and ionic liquid crystals (ILCs) have been used to imprint morphologies onto inorganic crystalline materials that would otherwise have a different morphology.^[123,160,209–213] The unifying aspect of these studies and many other results is that often sheetlike or platelike particles form when using ILs as the reaction medium even at elevated temperatures in the isotropic phase (which typically is referred to as non-ordered).

Indeed, a recent study suggests that ILs and ILCs have some remaining order in the form of short-range ordered smectic clusters even above the clearing point.^[214] This is interesting and potentially useful because such an observation implies that an ILC may template 2D structures although they are not in a clear smectic arrangement. Clearly, more data are needed on this subject but ILCs will likely become very useful tools for morphology control in particle formation reactions. In particular, ILs and ILCs appear to exhibit quite stable mesostructural features that extend to higher temperatures than in lyotropic mesophases. As a result, ILs and ILCs extend the usable temperature ranges for templating nanocrystal formation – this in turn should provide access to materials that are not accessible via templating using lyotropic mesophases.

Further on, ILs are highly ionic species and the constituent ions strongly interact with other ions and surfaces. As a result, a direct effect on the surfaces of the produced nanomaterials is likely. Indeed, we have recently demonstrated that the formation of CuS and CuCo₂S₄ from ILs produces a surprisingly high electrochemical surface area compared to the same

compounds made via other synthetic approaches.^[215] This indicates that ILs are not only efficient templates in an interesting temperature range but also that their specific ionic nature may be a tool to engineer surface details that may have an impact on catalytic reactions such as the oxygen (OER) or the hydrogen evolution reaction (HER). Again, the available datasets are far from complete and more work will be needed to (1) understand and (2) control such IL-surface interactions and their role in surface design.

A further point of interest is the concept of ionic liquid precursors (ILPs).^[123] ILPs can be designed to include a number of elements into one compound that can then be used to synthesize nanomaterials. This is particularly interesting when considering the synthesis of compounds with more complex compositions: suitable ILPs can be made to contain all metal ions needed for product formation and thus possibly also provide access to non-stoichiometric compounds that are not easily accessible otherwise.^[114,215] While this concept is just being established, we have recently demonstrated that a wide variety of ILPs with different metal/metal ratios and various metal/metal combinations are accessible.^[216] Clearly, following the concept recently demonstrated, these and other ILPs are attractive for the formation of (metal sulfide) nanoparticles with a highly flexible and potentially quite unusual composition.^[114]

Similar observations can also be made for the sulfur sources, not only for metal containing ILs. While there are sulfur sources available, ILs may also provide access to single source precursors with both the metal and sulfur being part of the IL. Examples that come to mind as sulfur containing IL components are thiosulfate or thiooxalate, which could at the same time provide the anion and the sulfur for the metal sulfide formation process. As a result, ILs are emerging as very useful tools for metal sulfide engineering and design.

Besides the chemical and structural aspects discussed so far, the advantages of microwave reactions in ILs should not be underestimated. While this is not a new concept and has been discussed throughout the text, microwave synthesis in ILs will continue to provide fast, efficient, and versatile approaches towards new inorganic nanomaterials.

6. Challenges for Industry

One of the obvious challenges in materials development is the laboratory-to-market bottleneck.^[217] Clearly, a large number of the articles cited and discussed so far claim an application potential, yet the respective particles or materials will not be developed all the way to a product. This observation is certainly not unique to the materials described here but as some of the authors of the current article are employees of the Fraunhofer Society (<https://www.fraunhofer.de/>), Germany's largest society for technology development and transfer, a few thoughts may be in order. So, let us ask the question "why are most of the nanoparticles published in the literature not making it into a product?"

To answer this question, several aspects, which are partly not even technology related, have to be considered. One

examples is the phase between research/invention and successful innovation, the so called "valley of death". While the valley of death is often attributed to a funding gap for the process of translating inventions into commercial products, there are also claims that the valley of death is more likely to be relevant for publicly funded research.^[218–220]

Emerging concepts like open innovation in science (OIS) may help to overcome this discrepancy for publicly funded research.^[221] Briefly summarized, OIS aims at making research more relevant and impactful by "[...] purposively enabling, initiating, and managing inbound, outbound, and coupled knowledge flows and (inter/transdisciplinary [...]) collaboration across organizational and disciplinary boundaries and along all stages of the scientific research process, from the formulation of research questions and the obtainment of funding or development of methods (i.e. conceptualization) to data collection, data processing, and data analyses (exploration and/or testing) and the dissemination of results through writing, translation into innovation, or other forms of codifying scientific insight (i.e. documentation)".^[221]

Besides these non-technological aspects, there clearly are also technology-related challenges that need to be overcome. The difficulty of technology transfer in nanoparticle synthesis and design is illustrated, e.g., by the fact that even after Park et al. published an astonishingly universal synthetic method for various ultra-fine metal and metal oxide nanoparticles (iron, iron oxide, cobalt oxide, manganese oxide) over a 40 g scale in 2004 and Hanhwa Chemical (now Hanwha Solutions), one of the biggest chemical companies in South Korea signed a memorandum of understanding (MOU) in 2008 on the technology transfer, there is no sign of mass production of such nanoparticles in the market yet.^[222] Size control and reproducibility of nanoparticles are the main issue of the production of them in a larger scale product.^[223] As the batch process is the commonly used synthetic method for nanoparticles, it is challenging to keep synthetic parameters, such as pressure,

temperature, reagent concentration, reaction time, heating rates, stirring speed, identical between each batch.

Additionally, a recent study by Jean et al. highlights some specific aspects of the commercialization of nanoparticles as exemplified by lead sulfide and perovskite nanoparticles.^[224] According to the authors, who used a Monte Carlo modeling study for evaluation, the overall cost of present-day quantum dots (QDs) production far exceeds economically viable ranges for photovoltaic devices. The authors calculated median costs of 11 to 59 \$ per g for PbS QDs and 73 \$ per g for CsPbI₃ QDs. Considering the performance, this results in 0.15 to 0.84 \$ per W for PbS (20 % efficient photovoltaic cell) and to 0.74 \$ per W in the case of CsPbI₃. Moreover, the preparation of the QD inks necessary for device preparation adds 6.3 \$ per g of QDs, which amounts to an additional 0.09 \$ per W. In total, the authors state that QDs cause up to 55 % of the price of the entire module. As a result, even roll-to-roll-processed modules remain much more expensive than conventional silicon modules. Overall, this study clearly shows that not the performance or the development of new materials is the limiting step in the production of competitive QD modules for photovoltaics but the cost. Although this study does not specifically address other fields it is clear that the same argument can be made for other areas as well. Figure 14 shows a summary of direct contributions to the cost of QDs as described in this study.

The challenges regarding batch processes and production costs are surprising considering that there are technical solutions available that can overcome these issues. For example, flow reactors eliminate many of the drawbacks of batch processing. Flow processes are easily scalable and reduce production costs significantly.^[225–227] More recently, flow reactors have even been combined with machine-learning tools to create an autonomous quantum dot synthesis bot, which can optimize these complex nanoparticle reactions very efficiently.^[228] Nevertheless, unless these technological developments themselves are able to cross the valley of death to evolve

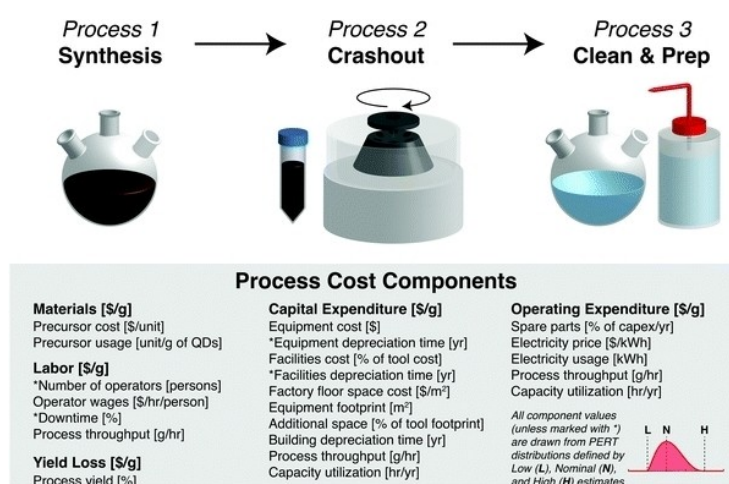


Figure 14. Monte Carlo cost modeling of colloidal QD synthesis. Each modeled process sequence consists of 3 distinct process steps: synthesis, crashout, and cleaning/preparation. Synthesis refers to the primary synthetic step (hot injection, heating up a precursor solution, or continuous flow synthesis). Crashout includes repeated precipitation and redispersal, characterization, and analysis of the QD product. Cleaning includes glassware cleaning and drying, followed by preparation for the next synthesis (degassing precursors and setting up equipment). Figure is from Jean et al., *Energy Environ. Sci.*, 2018, 11, 2295–2305.^[226] under the Open Access Attribution 3.0 Unported (CC BY 3.0).

into a commercially available technology, it is unlikely that they will carry technologies like the nanoparticles over the valley of death to make it into a product at the market.

Combined with the aspects mentioned in the beginning, that

- the research is maybe not relevant enough (e.g., it may not apply to a real world problem as specifically as viewed by the scientists) and needs significantly more development to be applicable,
- there is likely a funding gap for this further development,
- that funding gap might suppress entrepreneurial ambitions because of the high risk involved, and
- complementary, but necessary technologies are still not commercially available and still need development in their own right before commercialization,

this leads to very low chances of commercialization of the respective nanoparticle systems. OIS may be one approach to overcome certain aspects by helping to define more real-world problem-oriented research questions e.g. in co-creation processes together with society or industry, thus not only making the research more relevant from the beginning but also reducing the funding gap that will likely arise at the transition between laboratory and market.

7. Conclusions

In conclusion, metal sulfides are a broad and complex class of materials with a high application potential. As a result, metal sulfides have been studied intensely and new approaches and examples are coming out every week. The current article is a first attempt to highlight the power of ionic liquids for the synthesis of metal sulfides. Clearly, there are promising approaches, for example in microwave reactions, but IL-based metal sulfide synthesis is currently not fully developed and holds promise for further metal sulfide production strategies. This is not to be seen as an antagonistic approach with respect to existing methods. Rather, ILs offer pathways that complement more established routes and IL-based synthesis of metal sulfides thus holds promise for further advancing the functional (nano)materials research and development in conjunction with other approaches.

Acknowledgements

We thank Dr. Christina Günter (University of Potsdam) for help with SEM, EDX, and XRD, Dr. Andreas Bohn (Fraunhofer IAP) for help with TEM. The University of Potsdam (grant No. 53170000), the Deutsche Forschungsgemeinschaft (DFG, grants TA/571/13-1 & 13-2, WE 3696/1-1 & 1-2, KO4876/1-1 & 1-2, SPP 1708) are acknowledged for financial support.

Conflict of Interest

The authors declare no conflict of interest.

Keywords: Ionic liquids · ionic liquid crystals · ionic liquid precursors · metal sulfides · catalysis · electrochemistry · energy materials · LED · solar cells

- C.-H. Lai, M.-Y. Lu, L.-J. Chen, *J. Mater. Chem.* **2012**, *22*, 19–30.
- E. Sathiyaraj, S. Thirumaran, *Chem. Phys. Lett.* **2020**, *739*, 136972.
- W. Zhang, Z. Huang, H. Zhou, S. Li, C. Wang, H. Li, Z. Yan, F. Wang, Y. Kuang, *J. Alloys Compd.* **2020**, *816*, 152633.
- D. G. Moon, S. Rehan, D. H. Yeon, S. M. Lee, S. J. Park, S. Ahn, Y. S. Cho, *Sol. Energy Mater. Sol. Cells* **2019**, *200*, 109963.
- M. A. Green, *IEEE Trans. Electron Devices* **1984**, *31*, 671–678.
- S.-H. Hsu, C.-T. Li, H.-T. Chien, R. R. Salunkhe, N. Suzuki, Y. Yamauchi, K.-C. Ho, K. C.-W. Wu, *Sci. Rep.* **2015**, *4*, 6983. <https://doi.org/10.1038/srep06983>.
- A. C. Lokhande, K. V. Gurav, E. Jo, C. D. Lokhande, J. H. Kim, *J. Alloys Compd.* **2016**, *656*, 295–310.
- J. Jia, J. Wu, J. Dong, L. Fan, M. Huang, J. Lin, Z. Lan, *Chem. Commun.* **2018**, *54*, 3170–3173.
- J. Tirado, C. Roldán-Carmona, F. A. Muñoz-Guerrero, G. Bonilla-Arboleda, M. Ralaifarisoa, G. Grancini, V. I. E. Queloz, N. Koch, M. K. Nazeeruddin, F. Jaramillo, *Appl. Surf. Sci.* **2019**, *478*, 607–614.
- Y. Ma, P. Vashishtha, S. B. Shivarudraiah, K. Chen, Y. Liu, J. M. Hodgkiss, J. E. Halpert, *Sol. RRL* **2017**, *1*, 1700078.
- C. I. L. Santos, S. W. Machado, K. D. Wegner, L. A. P. Gontijo, J. Bettini, M. A. Schiavon, P. Reiss, D. Aldakov, *Nanomaterials* **2020**, *10*, 1252.
- M. G. Panthani, V. Akhavan, B. Goodfellow, J. P. Schmidtke, L. Dunn, A. Dodabalapur, P. F. Barbara, B. A. Korgel, *J. Am. Chem. Soc.* **2008**, *130*, 16770–16777.
- N. Naghavi, S. Spiering, M. Powalla, B. Cavana, D. Lincot, *Prog. Photovoltaics Res. Appl.* **2003**, *11*, 437–443.
- S. M. McLeod, C. J. Hages, N. J. Carter, R. Agrawal, *Prog. Photovoltaics Res. Appl.* **2015**, *23*, 1550–1556.
- B. Reeja-Jayan, A. Manthiram, *RSC Adv.* **2013**, *3*, 5412.
- C. Zhao, J. Wang, J. Jiao, L. Huang, J. Tang, *J. Mater. Chem. C* **2020**, *8*, 28–43.
- S. Günes, H. Neugebauer, N. S. Sariciftci, *Chem. Rev.* **2007**, *107*, 1324–1338. <https://doi.org/10.1021/cr050149z>.
- S. Dowland, T. Lutz, A. Ward, S. P. King, A. Sudlow, M. S. Hill, K. C. Molloy, S. A. Haque, *Adv. Mater.* **2011**, *23*, 2739–2744.
- C. Yang, Y. Sun, X. Li, C. Li, J. Tong, J. Li, P. Zhang, Y. Xia, *Nanoscale Res. Lett.* **2018**, *13*, 184.
- H. Bi, W. Zhao, S. Sun, H. Cui, T. Lin, F. Huang, X. Xie, M. Jiang, *Carbon N. Y.* **2013**, *61*, 116–123.
- Boon-P. on, S. Lien, T. Chang, J. Shi, M. Lee, *Prog. Photovoltaics Res. Appl.* **2020**, *28*, 328–341.
- S. Pitchaiya, M. Natarajan, A. Santhanam, V. M. Ramakrishnan, V. Asokan, P. Palanichamy, B. Rangasamy, S. Sundaram, D. Velauthapillai, *Mater. Lett.* **2018**, *221*, 283–288.
- M. S. G. Hamed, S. O. Oseni, A. Kumar, G. Sharma, G. T. Mola, *Sol. Energy* **2020**, *195*, 310–317.
- M. Marus, Y. Xia, H. Zhong, D. Li, S. Ding, U. Turavets, B. Xu, K. Wang, J. Zhang, X. W. Sun, *Appl. Phys. Lett.* **2020**, *116*, 191103.
- Y.-H. Won, O. Cho, T. T. Kim, D.-Y. Chung, T. T. Kim, H. Chung, H. Jang, J. Lee, D. Kim, E. Jang, *Nature* **2019**, *575*, 634–638.
- J.-H. Kim, H. Yang, *Chem. Mater.* **2016**, *28*, 6329–6335.
- Y. Huang, D. Xiong, X. Li, H. Maleki Kheimeh Sari, J. Peng, Y. Y. Li, Y. Y. Li, D. Li, Q. Sun, X. Sun, *Front. Chem.* **2020**, *8*.
- K. V. Kravchyk, R. Widmer, R. Erni, R. J.-C. Dubey, F. Krumeich, M. V. Kovalenko, M. I. Bodnarchuk, *Sci. Rep.* **2019**, *9*, 7988.
- Y. Zhou, D. Yan, H. Xu, J. Feng, X. Jiang, J. Yue, J. Yang, Y. Qian, *Nano Energy* **2015**, *12*, 528–537.
- S. Mei, C. J. Jafra, I. Laueremann, Q. Ran, M. Kärgell, M. Ballauff, Y. Lu, *Adv. Funct. Mater.* **2017**, *27*, 1701176.
- G. D. Park, S. H. Choi, J.-K. Lee, Y. C. Kang, *Chem. Eur. J.* **2014**, *20*, 12183–12189.
- A.-R. Park, K.-J. Jeon, C.-M. Park, *Electrochim. Acta* **2018**, *265*, 107–114.

- [33] M. Mao, L. Jiang, L. Wu, M. Zhang, T. Wang, *J. Mater. Chem. A* **2015**, *3*, 13384–13389.
- [34] Y. S. Jang, Y. C. Kang, *Phys. Chem. Chem. Phys.* **2013**, *15*, 16437.
- [35] J.-H. Zuo, Y.-J. Gong, *Tungsten* **2020**, *2*, 134–146.
- [36] H. Yang, B. Zhang, Y. Wang, K. Konstantinov, H. Liu, S. Dou, *Adv. Energy Mater.* **2020**, *10*, 2001764.
- [37] G. Kalimuldina, A. Nurpeissova, A. Adylkhanova, D. Adair, I. Taniguchi, Z. Bakenov, *ACS Appl. Energy Mater.* **2020**, acaem.0c01686.
- [38] G. L. Holleck, J. R. Driscoll, *Electrochim. Acta* **1977**, *22*, 647–655.
- [39] S. Xiao, X. Li, W. Sun, B. Guan, Y. Wang, *Chem. Eng. J.* **2016**, *306*, 251–259.
- [40] J. He, Y. Chen, A. Manthiram, *Adv. Energy Mater.* **2019**, *9*, 1900584.
- [41] Q. Pang, D. Kundu, L. F. Nazar, *Mater. Horiz.* **2016**, *3*, 130–136.
- [42] R. R. Chianelli, *Catal. Rev.* **1984**, *26*, 361–393.
- [43] R. R. Chianelli, M. Daage, M. J. Ledoux, in *Advances in Catalysis*, eds. D. D. Eley, H. Pines and W. O. Haag, Volume 40, **1994**, pp 177–232.
- [44] R. R. Chianelli, M. H. Siadati, M. P. De la Rosa, G. Berhaut, J. P. Wilcoxon, R. Bearden, B. L. Abrams, *Catal. Rev.* **2006**, *48*, 1–41.
- [45] S. Eijssbouts, S. W. Mayo, K. Fujita, *Appl. Catal. A* **2007**, *322*, 58–66.
- [46] Y. Guo, T. Park, J. W. Yi, J. Henzie, J. Kim, Z. Wang, B. Jiang, Y. Bando, Y. Sugahara, J. Tang, Y. Yamauchi, *Adv. Mater.* **2019**, *31*, 1807134.
- [47] P. Chen, N. Zhang, S. Wang, T. Zhou, Y. Tong, C. Ao, W. Yan, L. Zhang, W. Chu, C. Wu, Y. Xie, *Proc. Mont. Acad. Sci.* **2019**, *116*, 6635–6640.
- [48] E. Aslan, A. Sarilmaz, F. Ozel, I. Hatay Patir, H. H. Girault, *ACS Appl. Nano Mater.* **2019**, *2*, 7204–7213.
- [49] E. Hong, D. Kim, J. H. Kim, *J. Ind. Eng. Chem.* **2014**, *20*, 3869–3874.
- [50] K. Iwashina, A. Iwase, Y. H. Ng, R. Amal, A. Kudo, *J. Am. Chem. Soc.* **2015**, *137*, 604–607.
- [51] P. Chen, T. Zhou, M. Zhang, Y. Tong, C. Zhong, N. Zhang, L. Zhang, C. Wu, Y. Xie, *Adv. Mater.* **2017**, *29*, 1701584. <https://doi.org/10.1002/adma.201701584>.
- [52] A. Taubert, Z. Li, *Dalton Trans.* **2007**, No. 7, 723–727.
- [53] X. Kang, X. Sun, B. Han, *Adv. Mater.* **2016**, *28*, 1011–1030.
- [54] X. Duan, J. Ma, J. Lian, W. Zheng, *CrystEngComm* **2014**, *16*, 2550.
- [55] Y. Wang, Q. Hou, M. Ju, W. Li, *Nanomaterials* **2019**, *9*, 647.
- [56] Z. Li, Z. Jia, Y. Luan, T. Mu, *Curr. Opin. Solid State Mater. Sci.* **2008**, *12*, 1–8.
- [57] J. Stavek, M. Sipek, I. Hirasawa, K. Toyokura, *Chem. Mater.* **1992**, *4*, 545–555.
- [58] S. Libert, V. Gorshkov, V. Privman, D. Goia, E. Matijević, *Adv. Colloid Interface Sci.* **2003**, *100–102*, 169–183.
- [59] T. Trindade, J. D. P. de Jesus, P. O'Brien, *J. Mater. Chem.* **1994**, *4*, 1611.
- [60] C. B. Murray, D. J. Norris, M. G. Bawendi, *J. Am. Chem. Soc.* **1993**, *115*, 8706–8715.
- [61] B. O. Dabbousi, J. Rodriguez-Viejo, F. V. Mikulec, J. R. Heine, H. Mattoussi, R. Ober, K. F. Jensen, M. G. Bawendi, *J. Phys. Chem. B* **1997**, *101*, 9463–9475.
- [62] V. Perner, T. Rath, F. Pirolt, O. Glatter, K. Wewerka, I. Letofsky-Papst, P. Zach, M. Hobisch, B. Kunert, G. Trimmel, *New J. Chem.* **2019**, *43*, 356–363.
- [63] J. W. Thomson, K. Nagashima, P. M. Macdonald, G. A. Ozin, *J. Am. Chem. Soc.* **2011**, *133*, 5036–5041.
- [64] S. A. McCarthy, R. Ratkic, F. Purcell-Milton, T. S. Perova, Y. K. Gun'ko, *Sci. Rep.* **2018**, *8*, 2860.
- [65] B. Yuan, T. K. Egner, V. Venditti, L. Cademartiri, *Nat. Commun.* **2018**, *9*, 4078.
- [66] B. Heyne, K. Arlt, A. Geßner, A. F. Richter, M. Döblinger, J. Feldmann, A. Taubert, A. Wedel, *Nanomaterials* **2020**, *10*, 1858.
- [67] C. Xiong, M. Liu, X. Zhu, A. Tang, *Nanoscale Res. Lett.* **2019**, *14*, 19.
- [68] S. Jun, E. Jang, Y. Chung, *Nanotechnology* **2006**, *17*, 4806–4810.
- [69] H. Zhang, B.-R. Hyun, F. W. Wise, R. D. Robinson, *Nano Lett.* **2012**, *12*, 5856–5860.
- [70] J. O. Adeyemi, D. C. Onwudiwe, Hosten, E. C. Synthesis, *J. Mol. Struct.* **2019**, *1195*, 395–402.
- [71] J. Joo, H. B. Na, T. Yu, J. H. Yu, Y. W. Kim, F. Wu, J. Z. Zhang, T. Hyeon, *J. Am. Chem. Soc.* **2003**, *125*, 11100–11105.
- [72] J. Cui, L. Wang, X. Yu, *New J. Chem.* **2019**, *43*, 16007–16011.
- [73] A. J. Findlay, E. R. Estes, A. Gartman, M. Yücel, A. Kamyshny, G. W. Luther, *Nat. Commun.* **2019**, *10*, 1597.
- [74] K. D. Ikkurthi, S. Srinivasa Rao, M. Jagadeesh, A. E. Reddy, T. Anitha, H.-J. Kim, *New J. Chem.* **2018**, *42*, 19183–19192.
- [75] R. Bolagam, S. Um, *Coating* **2020**, *10*, 200.
- [76] H. Emadi, M. Salavati-Niasari, A. Sobhani, *Adv. Colloid Interface Sci.* **2017**, *246*, 52–74.
- [77] F. Xia, J. Zhou, J. Brugger, Y. Ngothai, O'Neill, B. G. Chen, A. Pring, *Chem. Mater.* **2008**, *20*, 2809–2817.
- [78] J. Moore, E. Nienhuis, M. Ahmadzadeh, J. McCloy, *AIP Adv.* **2019**, *9*, 035012. <https://doi.org/10.1063/1.5079759>.
- [79] W. Lojkowski, C. Leonelli, T. Chudoba, J. Wojnarowicz, A. Majcher, A. Mazurkiewicz, *Inorganics* **2014**, *2*, 606–619.
- [80] I. Bilecka, M. Niederberger, *Nanoscale* **2010**, *2*, 1358.
- [81] R. Souleyman, Z. Wang, C. Qiao, M. Naveed, C. Cao, *J. Mater. Chem. A* **2018**, *6*, 7592–7607.
- [82] S.-W. Hsu, C. Ngo, A. R. Tao, *Nano Lett.* **2014**, *14*, 2372–2380.
- [83] K. S. Suslick, G. J. Price, *Annu. Rev. Mater. Sci.* **1999**, *29*, 295–326.
- [84] G. Chatel, *Curr. Opin. Green Sustain. Chem.* **2019**, *15*, 1–6.
- [85] G.-J. Lee, J. J. Wu, *Powder Technol.* **2017**, *318*, 8–22.
- [86] L. Peng, X. Ji, H. Wan, Y. Ruan, K. Xu, C. Chen, L. Miao, J. Jiang, *Electrochim. Acta* **2015**, *182*, 361–367.
- [87] H. Hao, X. Lang, *ChemCatChem* **2019**, *11*, 1378–1393.
- [88] J.-S. Tsai, K. Dehvari, W.-C. Ho, K. Waki, J.-Y. Chang, *Adv. Mater. Interfaces* **2019**, *6*, 1801745.
- [89] S. Shen, Y. Zhang, L. Peng, B. Xu, Y. Du, M. Deng, H. Xu, Q. Wang, *CrystEngComm* **2011**, *13*, 4572.
- [90] I. Jen-La Plante, T. W. Zeid, P. Yang, T. Mokari, *J. Mater. Chem.* **2010**, *20*, 6612.
- [91] S. N. Shukla, P. Gaur, N. Rai, *Appl. Nanosci.* **2015**, *5*, 583–593.
- [92] J. H. L. Beal, P. G. Etchegoin, R. D. Tilley, *J. Phys. Chem. C* **2010**, *114*, 3817–3821.
- [93] P. Boudjouk, B. R. Jarabek, D. L. Simonson, D. J. Seidler, D. G. Grier, G. J. McCarthy, L. P. Keller, *Chem. Mater.* **1998**, *10*, 2358–2364.
- [94] P. Román, J. I. Beitia, Luque, A. Preparation, *Polyhedron* **1995**, *14*, 2925–2931.
- [95] M. Nowotny, S. Foro, S. Heinschke, R. C. Hoffmann, J. J. Schneider, *Eur. J. Inorg. Chem.* **2015**, *2015*, 512–519.
- [96] K. Ramasamy, M. A. Malik, P. O'Brien, J. Raftery, *Dalton Trans.* **2010**, *39*, 1460–1463.
- [97] N. Pradhan, B. Katz, S. Efrima, *J. Phys. Chem. B* **2003**, *107*, 13843–13854.
- [98] M. Al-Shakban, Z. Xie, N. Savjani, M. A. Malik, P. O'Brien, *J. Mater. Sci.* **2016**, *51*, 6166–6172.
- [99] A. Roffey, N. Hollingsworth, H.-U. Islam, W. Bras, G. Sankar, N. H. de Leeuw, G. Hogarth, *Nanoscale Adv.* **2019**, *1*, 2965–2978.
- [100] H.-U. Islam, A. Roffey, N. Hollingsworth, W. Bras, G. Sankar, N. H. de Leeuw, G. Hogarth, *Nanoscale Adv.* **2020**, *2*, 798–807.
- [101] A. Roffey, N. Hollingsworth, G. Hogarth, *Nanoscale Adv.* **2019**, *1*, 3056–3066.
- [102] J. Z. Mbese, P. A. Ajibade, *J. Sulfur Chem.* **2017**, *38*, 173–187.
- [103] S. A. Saah, N. O. Boadi, D. Adu-Poku, C. Wilkins, *R. Soc. Open Sci.* **2019**, *6*, 190943.
- [104] N. Pradhan, Efrima, S. Single-Precursor, *J. Am. Chem. Soc.* **2003**, *125*, 2050–2051.
- [105] Y. Zhang, J. Lu, S. Shen, H. Xu, Q. Wang, *Chem. Commun.* **2011**, *47*, 5226.
- [106] T. Tsuzuki and P. G. McCormick, *Nanostructured Mater.*, **1999**, *12*, 75–78.
- [107] J. V. Tolia, M. Chakraborty, Z. V. P. Murthy, *Part. Sci. Technol.* **2012**, *30*, 533–542.
- [108] Baláž, M. A. Zorkovská, F. Urakaev, Baláž, P. J. Briančin, Z. Bujňáková, M. Achimovičová, E. Gock, *RSC Adv.* **2016**, *6*, 87836–87842.
- [109] Z. Shalabayev, M. Baláž, N. Daneu, E. Dutková, Z. Bujňáková, M. Kaňuchová, Z. Danková, L. Balážová, F. Urakaev, L. Tkáčiková, M. Burkitbayev, *ACS Sustainable Chem. Eng.* **2019**, *7*, 12897–12909.
- [110] S. Anantharaj, S. R. Ede, K. Sakthikumar, K. Karthick, S. Mishra, S. Kundu, *ACS Catal.* **2016**, *6*, 8069–8097.
- [111] S. Chandrasekaran, L. Yao, L. Deng, C. Bowen, Y. Zhang, S. Chen, Z. Lin, F. Peng, P. Zhang, *Chem. Soc. Rev.* **2019**, *48*, 4178–4280.
- [112] A. C. Estrada, F. M. Silva, S. F. Soares, J. A. P. Coutinho, T. Trindade, *RSC Adv.* **2016**, *6*, 34521–34528.
- [113] Y. Kim, B. Heyne, A. Abouserie, C. Pries, C. Ippen, C. Günter, A. Taubert, A. Wedel, *J. Chem. Phys.* **2018**, *148*, 193818.
- [114] A. Abouserie, G. A. El-Nagar, B. Heyne, C. Günter, U. Schilde, M. T. Mayer, S. Stojkovič, C. Roth, A. Taubert, *ACS Appl. Mater. Interfaces* **2020**, *12*, 52560–52570.
- [115] N. A. García-Gómez, S. M. de la Parra-Arcieniega, L. L. Garza-Tovar, L. C. Torres-González, E. M. Sánchez, *J. Alloys Compd.* **2014**, *588*, 638–643.
- [116] Z. Li, A. Shkilnyy, A. Taubert, *Cryst. Growth Des.* **2008**, *8*, 4526–4532.
- [117] A. Taubert, C. Palivan, O. Casse, F. Gozzo, B. Schmitt, *J. Phys. Chem. C* **2007**, *111*, 4077–4082.

- [118] A. Abouserie, K. Zehbe, P. Metzner, A. Kelling, C. Günter, U. Schilde, P. Strauch, T. Körzdörfer, A. Taubert, *Eur. J. Inorg. Chem.* **2017**, 48, 5640–5649.
- [119] G. R. Lewis, *Chem. Commun.* **1998**, No. 17, 1873–1874.
- [120] C. K. Lee, K.-M. Hsu, C.-H. Tsai, C. K. Lai, I. J. B. Lin, *Dalton Trans.* **2004**, 4, 1120.
- [121] C. K. Lee, M. J. Ling, I. J. B. Lin, *Dalton Trans.* **2003**, 1, 4731–4737.
- [122] W. A. Herrmann, L. J. Goossen, G. R. J. Artus, C. Köcher, *Organometallics* **1997**, 16, 2472–2477.
- [123] A. Taubert, *Angew. Chem. Int. Ed.* **2004**, 43, 5380–5382; *Angew. Chem.* **2004**, 116, 5494–5496.
- [124] J. P. Hallett, T. Welton, *Chem. Rev.* **2011**, 111, 3508–3576.
- [125] M. Freemantle, *An Introduction to Ionic Liquids*; Royal Society of Chemistry, **2009**.
- [126] K. Zehbe, M. Kollosche, S. Lardong, A. Kelling, U. Schilde, A. Taubert, *Int. J. Mol. Sci.* **2016**, 17, 391.
- [127] R. Giermoth, *Angew. Chem. Int. Ed.* **2010**, 49, 2834–2839; *Angew. Chem.* **2010**, 122, 2896–2901.
- [128] A. P. Abbott, T. J. Bell, S. Handa, B. Stoddart, *Green Chem.* **2005**, 7, 705.
- [129] B. Dolling, A. L. Gillon, A. G. Orpen, J. Starbuck, X.-M. Wang, *Chem. Commun.* **2001**, 6, 567–568.
- [130] A. Angeloni, A. G. Orpen, *Chem. Commun.* **2001**, 4, 343–344.
- [131] M. W. Bouwkamp, E. Lobkovsky, P. J. Chirik, *J. Am. Chem. Soc.* **2005**, 127, 9660–9661.
- [132] M. Armand, F. Endres, D. R. MacFarlane, H. Ohno, B. Scrosati, *Nat. Mater.* **2009**, 8, 621–629.
- [133] T. Torimoto, T. Tsuda, K. I. Okazaki, S. Kuwabata, *Adv. Mater.* **2010**, 22, 1196–1221.
- [134] K. R. Seddon, *J. Chem. Technol. Biotechnol.*, **1997**, 68, 351–356.
- [135] E. F. Borra, O. Seddiki, R. Angel, D. Eisenstein, P. Hickson, K. R. Seddon, S. P. Worden, *Nature* **2007**, 447, 979–981.
- [136] O. Höfft, F. Endres, *Phys. Chem. Chem. Phys.* **2011**, 13, 13472.
- [137] S. Y. Kim, S. Kim, M. J. Park, *Nat. Commun.* **2010**, 1, 88.
- [138] E. Delahaye, R. Göbel, R. Löbbicke, R. Guillot, C. Sieber, A. Taubert, *J. Mater. Chem.* **2012**, 22, 17140.
- [139] K. Zehbe, A. Lange, A. Taubert, *Energy Fuels* **2019**, 33, 12885–12893.
- [140] D.-Y. Wang, C.-Y. Wei, M.-C. Lin, C.-J. Pan, H.-L. Chou, H.-A. Chen, M. Gong, Y. Wu, C. Yuan, M. Angell, Y.-J. Hsieh, Y.-H. Chen, C.-Y. Wen, C.-W. Chen, B.-J. Hwang, C.-C. Chen, H. Dai, *Nat. Commun.* **2017**, 8, 14283.
- [141] J. Ding, D. Zhou, G. Spinks, G. Wallace, S. Forsyth, M. Forsyth, D. MacFarlane, *Chem. Mater.* **2003**, 15, 2392–2398.
- [142] P. Wang, S. M. Zakeeruddin, I. Exnar, M. Grätzel, *Chem. Commun.* **2002**, 5, 2972–2973.
- [143] F. Fabregat-Santiago, J. Bisquert, E. Palomares, L. Otero, D. Kuang, S. M. Zakeeruddin, M. Grätzel, *J. Phys. Chem. C* **2007**, 111, 6550–6560.
- [144] N. V. Plechkova, K. R. Seddon, *Chem. Soc. Rev.* **2008**, 37, 123–150.
- [145] Z. Tshemese, M. D. Khan, S. Mlowe, N. Revaprasadu, *Mater. Sci. Eng. B* **2018**, 227, 116–121.
- [146] K. Biswas, C. N. R. Rao, *Chem. Eur. J.* **2007**, 13, 6123–6129.
- [147] T. Tsuzuki, J. Ding, P. G. McCormick, *Phys. B* **1997**, 239 (3–4), 378–387.
- [148] E. K. Goharshadi, S. H. Sajjadi, R. Mehrkhan, P. Nancarrow, *Chem. Eng. J.* **2012**, 209, 113–117.
- [149] M. Barzegar, A. Habibi-Yangjeh, M. Behboudnia, *J. Phys. Chem. Solids* **2010**, 71, 1393–1397.
- [150] Y. Jiang, Y. J. Zhu, *J. Phys. Chem. B* **2005**, 109, 4361–4364.
- [151] Y. Jiang, Y.-J. Zhu, *Chem. Lett.* **2004**, 33, 1390–1391.
- [152] M. Esmaili, A. Habibi-Yangjeh, *Phys. Status Solidi* **2009**, 206, 2529–2535.
- [153] T. Zhang, T. Doert, M. Ruck, *Z. Anorg. Allg. Chem.* **2017**, 643, 1913–1919.
- [154] L. Ge, X. Jing, J. Wang, S. Jamil, Q. Liu, D. Song, J. Wang, Y. Xie, P. Yang, M. Zhang, *Cryst. Growth Des.* **2010**, 10, 1688–1692.
- [155] Y. Fan, Y. Li, X. Han, X. Wu, L. Zhang, Q. Wang, *Molecules* **2019**, 24, 3776.
- [156] Y. Chen, C. Davoisne, J.-M. Tarascon, C. Guéry, *J. Mater. Chem.* **2012**, 22, 5295.
- [157] Y. Chen, J.-M. Tarascon, C. Guéry, *Electrochim. Acta* **2013**, 99, 46–53.
- [158] S. Murugesan, P. Kearns, K. J. Stevenson, *Langmuir* **2012**, 28, 5513–5517.
- [159] A. Taubert, I. Arbell, A. Mecke, P. Graf, *Gold Bull.* **2006**, 39, 205–211.
- [160] A. Taubert, P. Steiner, A. Manton, *J. Phys. Chem. B* **2005**, 109, 15542–15547.
- [161] H. T. Zhang, G. Wu, X. H. Chen, *Mater. Chem. Phys.* **2006**, 98, 298–303.
- [162] G. K. Veerasubramani, M.-S. Park, J.-Y. Choi, Y.-S. Lee, S. J. Kim, D.-W. Kim, *ACS Sustainable Chem. Eng.* **2019**, 7, 5921–5930.
- [163] L. Fatollahi, A. Feizbakhsh, E. Kono, H. A. Panahi, *J. Inorg. Organomet. Polym. Mater.* **2019**, 29, 80–86.
- [164] Y. Liu, M. Liu, M. T. Swihart, *Chem. Mater.* **2017**, 29, 4783–4791.
- [165] W. Zhang, Y. Wang, D. Zhang, S. Yu, W. Zhu, J. Wang, F. Zheng, S. Wang, J. Wang, *Nanoscale* **2015**, 7, 10210–10217.
- [166] M. Leonardi, M. Villacampa, J. C. Menéndez, *Chem. Sci.* **2018**, 9, 2042–2064.
- [167] W. B. McNamara, Y. T. Didenko, K. S. Suslick, *Nature* **1999**, 401, 772–775. <https://doi.org/10.1038/44536>.
- [168] C. O. Kappe, *Chem. Soc. Rev.* **2008**, 37, 1127.
- [169] E. R. Parnham, P. S. Wheatley, R. E. Morris, *Chem. Commun.* **2006**, No. 4, 380–382.
- [170] E. R. Parnham, R. E. Morris, *J. Mater. Chem.* **2006**, 16, 3682.
- [171] E. R. Parnham, R. E. Morris, *Acc. Chem. Res.* **2007**, 40, 1005–1013.
- [172] R. E. Morris, in *Studies in Surface Science and Catalysis*, eds. A. Gédéon, P. Massiani and F. Babonneau, Elsevier, Volume 174., 2008, pp. 33–42.
- [173] R. E. Morris, *Chem. Commun.* **2009**, No. 21, 2990.
- [174] K. Lu, Z. Zhu, L. Peng, H. Fu, X. Wang, E. Wang, *J. Coord. Chem.* **2020**, 73, 255–265.
- [175] H. Itoh, K. Naka, Y. Chujo, *J. Am. Chem. Soc.* **2004**, 126, 3026–3027.
- [176] K. E. Fox, N. L. Tran, T. A. Nguyen, T. T. Nguyen, P. A. Tran, *Surface Modification of Medical Devices at Nanoscale-Recent Development and Translational Perspectives In Biomaterials in Translational Medicine*; Elsevier, 2019; pp 163–189. <https://doi.org/10.1016/B978-0-12-813477-1.00008-6>.
- [177] I. Gurrappa, L. Binder, *Sci. Technol. Adv. Mater.* **2008**, 9, 043001.
- [178] W. Shockley, H. J. Queisser, *J. Appl. Phys.* **1961**, 32, 510–519.
- [179] J. P. Perdew, *Int. J. Quantum Chem.* **2009**, 28, 497–523.
- [180] J. M. Crowley, J. Tahir-Kheli, W. A. Goddard, *J. Phys. Chem. Lett.* **2016**, 7, 1198–1203.
- [181] P. Borlido, T. Aull, A. W. Huran, F. Tran, M. A. L. Marques, S. Botti, *J. Chem. Theory Comput.* **2019**, 15, 5069–5079.
- [182] A. Jain, S. P. Ong, G. Hautier, W. Chen, W. D. Richards, S. Dacek, S. Cholia, D. Gunter, D. Skinner, G. Ceder, K. Persson, *APL Mater.* **2013**, 1, 011002.
- [183] W. Li, C. F. J. Walther, A. Kuc, T. Heine, *J. Chem. Theory Comput.* **2013**, 9, 2950–2958.
- [184] J. Wang, Y. Wang, Y. Huang, W. J. G. M. Peijnenburg, J. Chen, X. Li, *RSC Adv.* **2019**, 9, 8426–8434.
- [185] B. Pan, X. Meng, Y. Xia, H. Lu, H. Li, *Phys. Chem. Chem. Phys.* **2020**, 22, 5735–5739.
- [186] C. C. Yang, Li, S. Size, *J. Phys. Chem. C* **2008**, 112, 2851–2856.
- [187] C. Wang, S. Chen, J.-H. Yang, L. Lang, H.-J. Xiang, X.-G. Gong, A. Walsh, S.-H. Wei, *Chem. Mater.* **2014**, 26, 3411–3417.
- [188] V. Havu, V. Blum, P. Havu, M. Scheffler, *J. Comput. Phys.* **2009**, 228, 8367–8379.
- [189] V. Blum, R. Gehrke, F. Hanke, P. Havu, V. Havu, X. Ren, K. Reuter, M. Scheffler, *Comput. Phys. Commun.* **2009**, 180, 2175–2196.
- [190] A. Togo, I. Tanaka, *Scr. Mater.* **2015**, 108, 1–5.
- [191] Z.-K. Liu, *J. Phase Equilib. Diffus.* **2009**, 30, 517–534.
- [192] L. Goerigk, S. Grimme, *Phys. Chem. Chem. Phys.* **2011**, 13, 6670.
- [193] J. P. Perdew, *Jacob's Ladder of Density Functional Approximations for the Exchange-Correlation Energy In AIP Conference Proceedings*; AIP, 2001; Vol. 577, pp 1–20. <https://doi.org/10.1063/1.1390175>.
- [194] V. Stevanović, S. Lany, X. Zhang, A. Zunger, *Phys. Rev. B* **2012**, 85, 115104.
- [195] C. R. A. Catlow, G. D. Price, *Nature* **1990**, 347, 243–248.
- [196] N. T. K. Thanh, N. Maclean, S. Mahiddine, *Chem. Rev.* **2014**, 114, 7610–7630.
- [197] J. Lee, J. Yang, S. G. Kwon, T. Hyeon, *Nat. Rev. Mater.* **2016**, 1, 16034.
- [198] J. Polte, *CrystEngComm* **2015**, 17, 6809–6830.
- [199] H. Cölfen, *Nat. Mater.* **2010**, 9, 960–961.
- [200] R. P. Swatloski, S. K. Spear, J. D. Holbrey, R. D. Rogers, *J. Am. Chem. Soc.* **2002**, 124, 4974–4975.
- [201] D. M. Phillips, L. F. Drummy, D. G. Conrady, D. M. Fox, R. R. Naik, M. O. Stone, P. C. Trulove, H. C. De Long, R. A. Mantz, *J. Am. Chem. Soc.* **2004**, 126, 14350–14351.
- [202] J. Richter, M. Ruck, *RSC Adv.* **2019**, 9, 29699–29710.
- [203] A. P. Abbott, G. Frisch, J. Hartley, K. S. Ryder, *Green Chem.* **2011**, 13, 471.
- [204] A. Salama, M. Neumann, C. Günter, A. Taubert, *Beilstein J. Nanotechnol.* **2014**, 5, 1553–1568.

- [205] R. F. P. Pereira, K. Zehbe, C. Günter, T. dos Santos, S. C. Nunes, F. A. A. Paz, M. M. Silva, P. L. Granja, A. Taubert, V. de Zea Bermudez, *ACS Omega* **2018**, *3*, 10811–10822.
- [206] K. Goossens, K. Lava, C. W. Bielawski, K. Binnemans, *Chem. Rev.* **2016**, *116*, 4643–4807.
- [207] K. Binnemans, *Chem. Rev.* **2005**, *105*, 4148–4204.
- [208] L. Douce, J.-M. Suisse, D. Guillon, A. Taubert, *Liq. Cryst.* **2011**, *38*, 1653–1661.
- [209] W. Dobbs, J.-M. Suisse, L. Douce, R. Welter, *Angew. Chem.* **2006**, *118*, 4285–4288.
- [210] Q. Qin, G. Zhang, Z. Chai, J. Zhang, Y. Cui, T. Li, W. Zheng, *Nano Energy* **2017**, *41*, 780–787.
- [211] T. Ban, Y. Kondo, Y. Ohya, *CrystEngComm* **2016**, *18*, 8731–8738.
- [212] T. Chen, Z. Xie, W. Jiang, W. Jiang, X. Zhang, J. Liu, *J. Adv. Ceram.* **2016**, *5*, 111–116.
- [213] Z. Li, Z. Liu, J. Zhang, B. Han, J. Du, Y. Gao, T. Jiang, *J. Phys. Chem. B* **2005**, *109*, 14445–14448.
- [214] M. C. Schlick, N. Kapernaum, M. M. Neidhardt, T. Wöhrle, Y. Stöckl, S. Laschat, F. Giesselmann, *ChemPhysChem* **2018**, *19*, 2305–2312.
- [215] A. Abouserie, U. Schilde, A. Taubert, *Z. Kristallogr. New Cryst. Struct.* **2018**, *233*, 743–746.
- [216] C. Balischiwski, K. Behrens, K. Zehbe, C. Guenter, S. Mies, E. Sperlich, A. Taubert, A. Kelling, *Chem. Eur. J.* **2020**.
- [217] Y. Shiga, N. Umezawa, N. Srinivasan, S. Koyasu, E. Sakai, M. Miyauchi, *Chem. Commun.* **2016**, *52*, 7470–7473.
- [218] J. Hudson, H. F. Khazragui, *Drug Discovery Today* **2013**, *18*, 610–613.
- [219] J. B. Klitsie, R. A. Price, C. S. H. De Lille, *Des. Manag. J.* **2019**, *14*, 28–41.
- [220] T. R. Beard, G. S. Ford, T. M. Koutsky, L. J. Spiwak, *Res. Eval.* **2009**, *18*, 343–356.
- [221] S. Beck, C. Bergenholtz, M. Bogers, T.-M. Bresseur, M. L. Conradsen, D. Di Marco, A. P. Distel, L. Dobusch, D. Dörler, A. Effert, B. Fecher, *Ind. Innov.* **2020**, 1–50.
- [222] J. Park, K. An, Y. Hwang, J.-G. Park, H.-J. Noh, J.-Y. Kim, J.-H. Park, N.-M. Hwang, T. Hyeon, *Nat. Mater.* **2004**, *3*, 891–895.
- [223] O. Długosz, M. Banach, *React. Chem. Eng.* **2020**, *5*, 1619–1641.
- [224] J. Jean, J. Xiao, R. Nick, N. Moody, M. Nasilowski, M. Bawendi, V. Bulović, *Energy Environ. Sci.* **2018**, *11*, 2295–2305.
- [225] D. Ness, J. Niehaus, V.-H. Tran, H. Weller, *MRS Proc.* **2012**, *1386*, mrsf11-1386-d07-02.
- [226] H. Weller, J. Niehaus, *Reactor for the Manufacture of Nanoparticles*. US9084979B2, **2011**.
- [227] H. L. Hellstern, J. Becker, P. Hald, M. Bremholm, A. Mamakhel, B. B. Iversen, *Ind. Eng. Chem. Res.* **2015**, *54*, 8500–8508.
- [228] R. W. Epps, M. S. Bowen, A. A. Volk, Abdel-K. Latif, S. Han, K. G. Reyes, A. Amassian, M. Abolhasani, *Adv. Mater.* **2020**, *32*, 2001626.
- [229] W. Liu, H. Niu, J. Yang, K. Cheng, K. Ye, K. Zhu, G. Wang, D. Cao, J. Yan, *Chem. Mater.* **2018**, *30*, 1055–1068.
- [230] X. Rui, H. Tan, Q. Yan, *Nanoscale* **2014**, *6*, 9889–9924.
- [231] G. Wang, L. Zhang, J. Zhang, *Chem. Soc. Rev.* **2012**, *41*, 797–828.

Manuscript received: December 18, 2020

Revised manuscript received: February 12, 2021